Cytoarchitectonic mapping of attentional selection and reorienting in parietal cortex

Céline R. Gillebert[a], Dante Mantini[b], Ronald Peeters[c], Patrick Dupont[a], Rik Vandenberghe[a,d]
[a]Laboratory for Cognitive Neurology, KU Leuven; [b]Laboratory for Neuro- and Psychophysiology, KU Leuven; [c]Radiology Department, University Hospitals Leuven; [d]Neurology Department, University Hospitals Leuven, Leuven, Belgium

Correspondence to: Rik Vandenberghe. Neurology Department, University Hospitals Leuven, Herestraat 49 - box 7003, 3000 Leuven, Belgium. Phone: +3216344280, Fax: +3216344285. E-mail: `rik.vandenberghe@uz.kuleuven.ac.be`.

This is a pre-copy-editing, author-produced PDF of an article accepted for publication in NeuroImage *following peer review. The definitive publisher-authenticated version (**Gillebert, C.R., Mantini, D., Peeters, R., Dupont, P., and Vandenberghe, R. (2013). Cytoarchitectonic mapping of attentional selection and reorienting in parietal cortex. NeuroImage, 67:257-272**) is available online at: http://dx.doi.org/10.1016/j.neuroimage.2012.11.026.*

Abstract

Selection and reorienting are two fundamental aspects of spatial attention. By means of event-related fMRI in a total of 26 subjects, we localised these two processes within a same experiment applying a probabilistic cytoarchitectonic reference frame. In a classical spatial cueing paradigm, the target was presented at the cued location either alone (60% of trials) or in combination with a contralateral distracter ('competition trials', 20% of trials), or at a location opposite to the cued location ('invalidly cued trials', 20% of trials). In a sensory control experiment we differentiated between the attentional and the sensory effects of the distracter. In areas hIP1 and hIP3, competition trials exerted a significantly stronger attentional effect than invalidity trials. Conversely, area PF in the right hemisphere showed an invalidity effect in the absence of competition effect. A third type of response was found in areas PFm and PGa which showed both an invalidity and a competition effect. The combined study of selection and reorienting using a cytoarchitectonic reference frame enabled us to resolve the wide between-study variance in temporoparietal coordinates associated with the invalidity effect. Furthermore, the study demonstrated within a same experiment a functional dissociation between reorienting and selection in parietal cortex.

Keywords

spatial cueing, invalidity, biased competition, intraparietal sulcus, temporoparietal junction

Abbreviations

ANOVA, analysis-of-variance; DTI: diffusion tensor imaging; EPI, echoplanar images; fMRI, functional magnetic resonance imaging; FWHM, full-width at half-maximum; G-G, Greenhouse-Geisser; GLM, general linear model; IPL, inferior parietal lobule; IPS, intraparietal sulcus; MNI, Montreal Neurological Institute; MPM, maximum probability map; TPJ, temporoparietal junction; SENSE, sensitivity encoding; RT, reaction time; TE, echo time; TR, repetition time; SPL, superior parietal lobule; VOI, volume-of-interest

1 Introduction

Functional specialization and integration within parietal cortex during spatial attentional processing is a topic of high relevance, both from a cognitive neuroscience and applied clinical perspective (Bays et al., 2010; Corbetta and Shulman, 2011; Posner, 2012; Vandenberghe et al., 2012). Converging evidence from functional magnetic resonance imaging (fMRI) and patient studies suggests a functional dissociation between attentional reorienting and attentional selection. The canonical spatial cueing paradigm with valid and invalid cues (Corbetta et al., 2005; Gillebert et al., 2011; Nobre et al., 1997; Posner et al., 1980, 1984; Rafal, 1998; Vandenberghe et al., 2012) activates the intraparietal sulcus (IPS) (Corbetta et al., 1993, 2000; Giesbrecht et al., 2003; Hopfinger et al., 2000; Kastner et al., 1999; Kim et al., 1999; Nobre et al., 1997; Woldorff et al., 2004), with additional involvement of the right temporoparietal junction (TPJ), in particular when subjects reorient towards the target location after an invalid spatial cue (Arrington et al., 2000; Corbetta et al., 2000; Kincade et al., 2005; Vossel et al., 2006). When subjects covertly attend to a peripheral target, adding a distracter to the display enhances activity in the middle (horizontal) segment of IPS (Gillebert et al., 2012a; Molenberghs et al., 2008; Vandenberghe et al., 2005). In a series of sensory control experiments involving 12 (Molenberghs et al., 2008), 16 (Vandenberghe et al., 2005), and 22 (Gillebert et al., 2012a) volunteers, respectively, this activity increase was absent under central attention conditions, resulting in a significant interaction between task (central versus peripheral attention) and stimulus display (single versus double peripheral stimulation) (Vandenberghe et al., 2005; Gillebert et al., 2012a). These findings implicate the middle IPS in selection between competing stimuli (Bundesen, 1990; Desimone and Duncan, 1995; Vandenberghe and Gillebert, 2009).

From a neuroanatomical perspective, denotations such as TPJ and middle or horizontal IPS segment are unsatisfactory since they miss the cytoarchitectonic and connectionist demarcations that one would traditionally require for definition of functionally specialised areas (Felleman and Van Essen, 1991; Orban and Vanduffel, 2007). As a consequence, the coordinates subsumed under the term "TPJ", for example, are widely dispersed between studies (Corbetta et al., 2008; Decety and Lamm, 2007; Mars et al., 2012). Furthermore, macroanatomical landmarks are variable across individuals and often do not match borders of cytoarchitectonic areas (Amunts and Zilles, 2001; Zilles et al., 2002). A clear demarcation between subregions within the parietal cortex is therefore impossible based on anatomical landmarks alone (Caspers et al., 2008). To overcome these problems, observer-independent probabilistic mapping procedures have been developed based on statistical analysis of the laminar cell-body distributions in sections of postmortem brains (Schleicher et al., 1999). For each voxel, the probability is given by the number of postmortem brains in whom the voxel belongs to that area divided by the total number of brains examined (e.g. 10 in the case of the Jülich-Düsseldorf cytoarchitectonic atlas) (Amunts and Zilles, 2001; Zilles et al., 2002). In the Maximum Probability Map (MPM), each voxel is assigned to the cytoarchitectonic area that it most likely belongs to (Eickhoff et al., 2005, 2006). These cytoarchitectonic maps registered to a standard space with proper estimates of between-subjects variability have been made available to the scientific community (Eickhoff et al., 2005) and have proven their utility e.g. in studies of mathematical cognition (Rosenberg-Lee et al., 2011; Wu et al., 2009). Usage of a cytoarchitectonic probabilistic map in standard space may also enhance comparability between studies (Eickhoff et al., 2005, 2006, 2007). It offers the further advantage that for functional interrogation areas of interest can be defined in a way that is independent of their functional activity levels.

According to the most recent cytoarchitectonic analysis, inferior and superior parietal cortex can be parcellated in 17 distinct areas. Three such areas, hIP1 (Choi et al., 2006), hIP2 (Choi et al., 2006) and hIP3 (Choi et al., 2006; Scheperjans et al., 2008a,b) belong to the intraparietal sulcus, the angular gyrus contains two cytoarchitectonic areas (PGp, PGa), 5 belong to the supramarginal gyrus (PFt, PFop, PFcm, PF, PFm) (Caspers et al., 2006, 2008) and 7 to the

superior parietal lobe (SPL) (5L, 5M, 5Ci, 7A, 7P, 7M, 7PC) (Scheperjans et al., 2008a,b) (Fig. 1). Using this reference frame (Caspers et al., 2006, 2008; Choi et al., 2006; Scheperjans et al., 2008a,b) and a hybrid spatial cueing paradigm (Gillebert et al., 2011), in which the expectancy rate of competition and invalid trials was matched, we directly compared activity levels during attentional selection and reorienting.

2 Material and Methods

2.1 Subjects

We conducted 3 fMRI experiments in a total of 26 healthy volunteers. Subjects were strictly right-handed, reported normal or corrected-to-normal vision, were free of psychotropic and vasoactive medication and had no neurologic or psychiatric history. Sixteen subjects participated in the main experiment (8 women/8 men, aged 20-26 years) and 4 of them (3 women/1 man, aged 20-24 years) also in a sensory control experiment. In addition, we obtained resting-state fMRI data in a group of 16 subjects (8 women/8 men, aged 20-31 years), 6 of whom also participated in the main experiment. All subjects gave written informed consent in accordance with the Declaration of Helsinki. The study was approved by the Ethics Committee of the University Hospitals Leuven.

2.2 Stimuli and experimental paradigm

Stimulus presentation and response registration were controlled by a PC running Presentation 11.3 (Neurobehavioral systems, Albany, CA). Stimuli were projected onto a translucent screen in front of the subject during scanning by means of a liquid crystal display projector (1024×768 pixels; Barco 6400i; Barco, Kortrijk, Belgium). Eye movements were registered using an Applied Science Laboratory infrared system (ASL 5000/LRO system; Waltham, MA) and stored for subsequent analysis.

2.2.1 Main experiment

Each trial started with a temporal warning cue (duration 150 ms), followed by a central spatial arrow pointing leftward or rightward (200 ms), a delay phase (200 ms) during which only the fixation dot was shown, and a test phase during which a peripheral grating was presented (200 ms, size 3.5°, 0.5 cycles/degree, mean luminance, 19.2 cd/m^2) to the left or to the right at 7.6° eccentricity on the horizontal meridian (Fig. 2A). Participants held a response box in their right hand, and were instructed to select a key press as a function of the target orientation. The target was rotated clockwise or counter-clockwise with respect to a 45° reference orientation. Per run and per condition, these two alternatives occurred with equal frequency. The orientation difference (relative to 45°) was identical across all trial types. It was adapted on-line from run to run to obtain an average performance level of 85% correct.

In 60% of the trials a single grating appeared at the cued location ('valid cue/single left target', 'valid cue/single right target'), in 20% of the trials a single grating appeared contralaterally to the cued location ('invalid cue/left target', 'invalid cue/right target'), and in the remaining 20% the target grating appeared at the cued location together with a contralateral irrelevant grating ('bilat. stim./left target', 'bilat. stim./right target') (Fig. 2B). The distracter orientation, rotated clockwise or counter-clockwise relative to 45°, was pseudorandomly chosen with the constraint that each option occurred equally often and that it was congruent with the target orientation in half of trials and incongruent in the remaining half.

Each participant performed 840 task trials in total, divided into 6 runs of 140 trials. In each run, task trials were intermixed with 28 null events. The event sequence was optimized for the contrast of 'invalid cue' trials versus 'valid cue/single target' trials, and for the contrast of 'bilat.

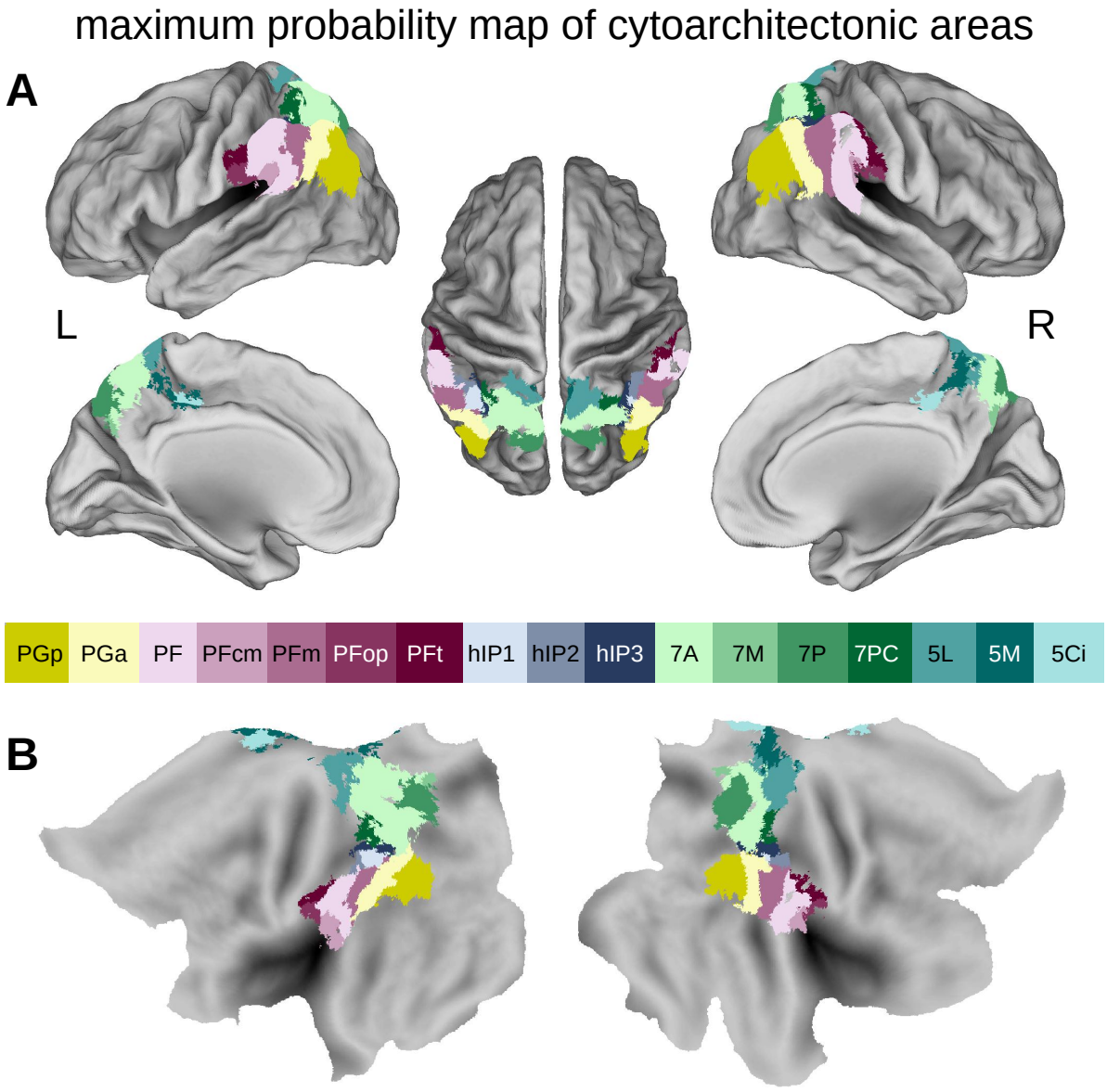

Figure 1 – **Maximum probability maps of cytoarchitectonic areas in parietal cortex** Maximum probability map (Eickhoff et al., 2005, 2006) of cytoarchitectonic areas covering the inferior parietal cortex (PGp, PGa, PF, PFcm, PFm, PFop, PFt), the intraparietal sulcus (hIP1, hIP2, hIP3), and the superior parietal lobule (5L, 5M, 5Ci, 7A, 7M, 7PC, 7P) (Caspers et al., 2006; Choi et al., 2006; Scheperjans et al., 2008a,b). The maximum probability map is projected onto (**A**) a surface rendering of the brain (lateral, medial and dorsal view) and (**B**) on the flattened brain surface [Population-Average, Landmark- and Surface-based (PALS) Atlas, Caret 5.612 (Van Essen, 2005)].

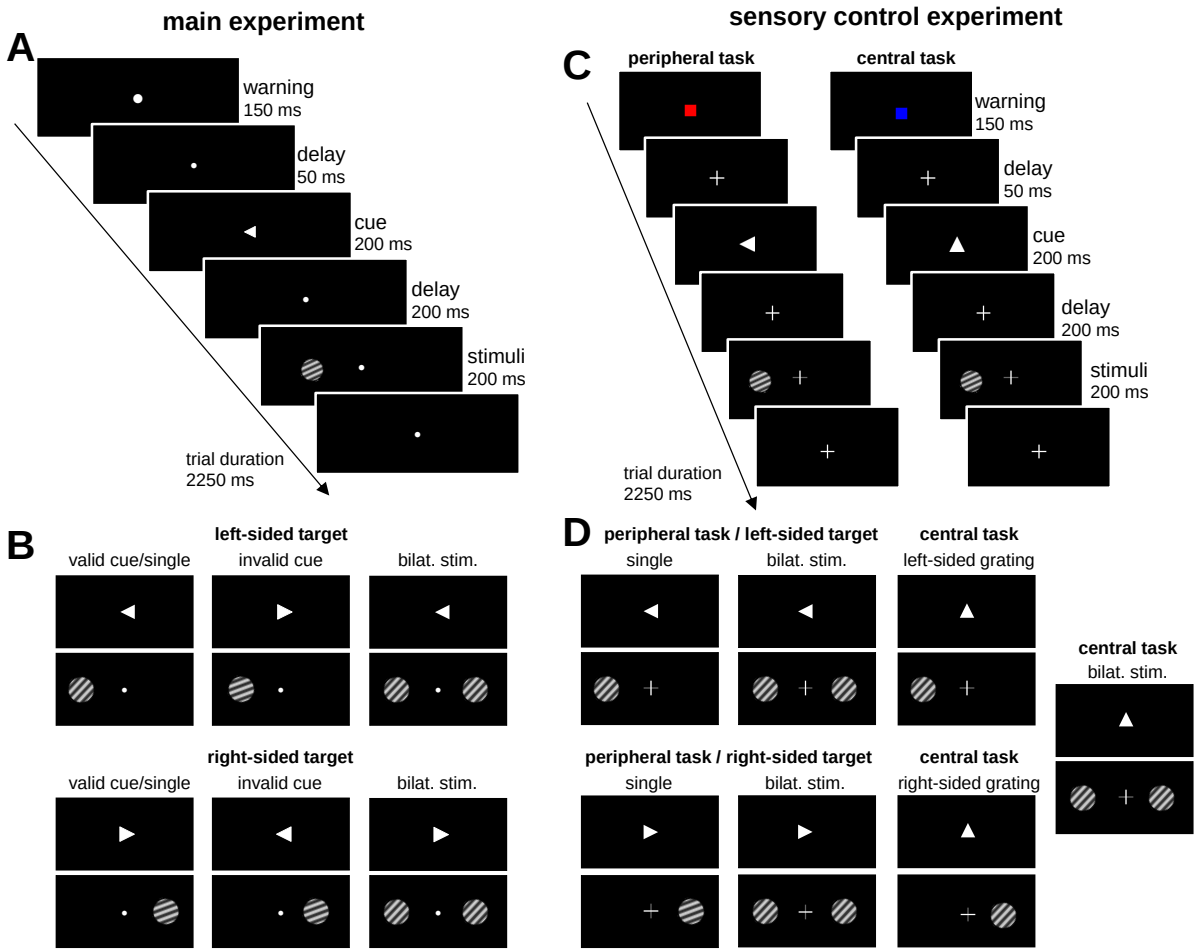

Figure 2 – **Experimental paradigm** (**A-B**) Main experiment. (**A**) Example of the trial sequence: A central cue pointed to the left or the right visual field. After a delay, a target grating was presented. Subjects were instructed to make a key press depending on the orientation of the target grating relative to a reference orientation of 45°. (**B**) Illustration of the 2×3 experimental design with target location (left-sided, right-sided) and task condition (valid cue/single target, invalid cue, bilat. stim.) as factors. (**C-D**) Sensory control experiment. (**C**) Example of the trial sequence. (**D**) Illustration of the 2×2 experimental design with task (peripheral attention, central attention) and stimulus display (single stim., bilat. stim.) as factors.

stim.' versus 'valid cue/single target' trials (Wager and Nichols, 2003). Before the scanning session, each participant practiced the task outside the scanner (1 run of 140 trials), based on which we determined the orientation difference to be discriminated in the first scanning run.

2.2.2 Sensory control experiment

The experiment had a 2×2 factorial design, with task ('peripheral attention', 'central attention') and stimulus display ('single stim.', 'bilat. stim.') as factors (Fig. 2C-D). In a mixed design, blocks of peripheral attention alternated with blocks of central attention. The total duration of each block was 54 s. Each block started with a written instruction ('peripheral' or 'central') (2250 ms) followed by a delay during which only a fixation cross was shown (2250 ms), and 18 experimental trials intermixed with 4 null events. Each trial (duration 2250 ms) started with an instructive color cue (150 ms), reminding the subjects of the initial instruction of the block they were in (Fig. 2C). The color, red or blue, indicated whether participants had to discriminate the orientation of the spatially cued peripheral grating (peripheral task) or, alternatively, conduct a central dimming detection task (central task). After a 50 ms delay, the color cue was followed by a central arrow cue (200 ms). In the peripheral attention blocks, the

arrow pointed either rightward or leftward. It was always valid. Following a delay (200 ms) during which only the fixation cross was shown, a peripheral grating was presented for 200 ms at 7.6° eccentricity on the horizontal meridian to the left or the right (test phase). The target grating was presented on its own ('valid cue/single left target', 'valid cue/single right target') or together with a contralateral distracter ('bilat. stim./left target', 'bilat. stim./right target') (Fig. 2D). Concomitantly, the luminance of either the horizontal or vertical bar of the fixation cross dimmed. In the peripheral attention blocks, subjects had to press a key depending on the orientation of the cued grating. In the central attention blocks, subjects had to press a key depending on which bar of the fixation cross dimmed (Fig. 2C). In the central attention block trials, the arrow cue invariably pointed upwards but the sensory input was otherwise strictly matched between the peripheral and the central task trials. The orientation difference (relative to 45°) and the degree of dimming were adapted on-line from run to run to obtain an average performance level of 85% correct in the peripheral orientation discrimination and central luminance dimming task, respectively.

Each peripheral attention block contained 7 'valid cue/single left target' and 7 'valid cue/single right target' trials, 2 'bilat. stim./left target' and 2 'bilat. stim./right target' trials. Each central attention block contained 7 'central task/single left stim.' trials, 7 'central task/single right stim.' trials and 4 'central task/bilat. stim.' trials. In addition to the 18 experimental trials each block also contained 4 null events. Participants performed 6 runs in totals. The order of the blocks was counterbalanced between runs. Before the scanning session, each participant practiced the task outside the scanner (1 training session of 192 trials), based on which we determined the orientation difference to be discriminated and the degree of dimming to be detected in the first scanning run.

2.2.3 Resting-state fMRI experiment

During the resting-state fMRI experiment, subjects were instructed to remain awake with their eyes closed and not to think about anything in particular for the duration of the scan (425 s).

2.3 Image acquisition

The fMRI experiments were run in a 3T Philips Intera magnet with an eight-channel sensitivity encoding (SENSE) head coil. The whole-brain functional scans consisted of T_2*-weighted gradient-echo echoplanar images (EPI) acquired continuously in an ascending order (6 time series, 189 scans per time series in the main experiment, 216 scans per time series in the sensory control experiment, 2000 ms repetition time (TR), 30 ms echo time (TE), 80×80 acquisition matrix, 2.75×2.75 mm^2 in-plane resolution, 36 3.75 mm thick axial slices without gap). During the resting-state fMRI run, we acquired 250 whole-brain scans with 1700 ms TR, 33 ms TE, 90° flip angle, 64×64 acquisition matrix, 3.59×3.59 mm^2 in-plane resolution, 4 mm slice thickness without gap and 32 axial slices covering the whole brain. In each subject, we also acquired a T_1-weighted anatomical image (9.6 ms TR, 4.6 ms TE, 256×256 acquisition matrix, 1×1 mm^2 in-plane resolution, 182 1.2 mm thick coronal slices).

2.4 Analysis of behavioral data

For each subject and each condition in the experimental design, we calculated two measures of performance: d' (MacMillan and Creelman, 1991), the ability to discriminate between two grating orientations, and the average reaction time (RT) on correct trials. Data in the main experiment were analyzed using a repeated measures analysis-of-variance (ANOVA) with task condition (valid cue/single target, invalid cue, bilat. stim.) and target location (left target, right target) as factors. When sphericity could not be assumed (Mauchly's sphericity test: $P<0.05$), P-values were adjusted using the Greenhouse-Geisser correction (G-G adj.). Posthoc

comparisons included the pairwise comparisons between different task conditions (threshold: $P<0.05$, Bonferroni-corrected for multiple comparisons). Data in the sensory control experiment were analyzed using a repeated measures ANOVA with task (peripheral task, central task) and stimulus display (single stim., bilat. stim.) as factors. Given the low sample size, the latter analysis was performed using a fixed effects model, with one datapoint per condition and per run (24 runs in total).

To analyze eye movements, we defined a region of interest that covered a rectangular area in the left and right visual field from 1° to 10° eccentricity. Deviations of eye movements into the regions of interest were detected automatically and calculated. For the main experiment, deviations of eye movements into the regions of interest were submitted to a repeated measures ANOVA with task condition (3 levels: valid cue/single target, invalid cue, bilat. stim.) and target location (2 levels: left target, right target) as factors. For the sensory control experiment, deviations of eye movements into the regions of interest were submitted to a fixed effects repeated measures ANOVA with task (2 levels: central task, peripheral task) and stimulus display (2 levels: single stim., bilat. stim.) as factors.

2.5 Preprocessing

Preprocessing and statistical analysis were carried out with Statistical Parametric Mapping 5 (Wellcome Trust Centre for Neuroimaging, London, UK, `http://www.fil.ion.ucl.ac.uk/spm`). Cytoarchitectonic mapping was based on the probabilistic brain atlas (Jülich-Düsseldorf cytoarchitectonic atlas), using the Anatomy Toolbox (`http://www.fz-juelich.de/inm/inm-1/DE/Forschung/_docs/SPMAnatomyToolbox/SPMAnatomyToolbox_node.html`) (Eickhoff et al., 2005, 2006, 2007).

The EPI images were corrected for differences in acquisition time, realigned to correct for head movements and co-registered to the T_1-weighted image. The T_1-weighted image was warped into the Montreal Neurological Institute (MNI) space using the unified segmentation approach of SPM5 (Ashburner and Friston, 2005) and the resulting transformation was used to spatially normalize the functional images. The voxel size of the images in MNI space was $3\times3\times3$ mm^3.

2.6 Volume-of-interest based analysis

2.6.1 Task-related fMRI

Data from the fMRI main experiment were analyzed using a random effects general linear model (GLM) with 6 regressors corresponding to each of the experimental conditions (Fig. 2B) plus 6 motion regressors. We analyzed the data from the sensory control experiment using a fixed effects GLM. The regressors consisted of the 4 peripheral attention conditions, the 3 central attention conditions (Fig. 2D) and the 6 motion regressors. The hemodynamic response was modeled using the canonical hemodynamical response function in SPM without temporal derivatives.

To characterize cytoarchitectonic areas functionally, we defined volumes-of-interest (VOIs) based on the 17 cytoarchitectonic areas in parietal cortex (Caspers et al., 2006, 2008; Choi et al., 2006; Scheperjans et al., 2008a,b) independently of any activity map (Fig. 3). For each cytoarchitectonic area we included only those voxels in the VOI with a probability class of $\geq 90\%$. As a second criterion, we required each VOI to contain at least 29 voxels, i.e. the product of twice the full-width at half-maximum (FWHM) of the intrinsic resolution of the fMRI data in each direction. If necessary, the probability threshold was lowered for a given cytoarchitectonic VOI until this minimum size was reached (Table 1). The voxels included in these cytoarchitectonic VOIs therefore represent the 'centre' or 'core' of the probabilistic map corresponding to the cytoarchitectonic areas (Fig. 3). Next, we characterized the cytoarchitectonic VOIs functionally.

For this analysis, no smoothing was applied to the fMRI data. For each VOI, we calculated the ratio between the signal change in each of the conditions and the mean signal over the entire run, averaged over all voxels belonging to that VOI (Eickhoff et al., 2005). We evaluated in each VOI the following contrasts using one-sample t-tests:

- contrast 1, main experiment: [('bilat. stim./left target' + 'bilat. stim./right target') – ('valid cue/single left target' + 'valid cue/single right target')]
- contrast 2, main experiment: [('invalid cue/left target' + 'invalid cue/right target') – ('valid cue/single left target' + 'valid cue/single right target')]
- contrast 3, main experiment: [('bilat. stim./left target' + 'bilat. stim./right target') – ('invalid cue/left target' + 'invalid cue/right target')], and the reverse
- contrast 4, sensory control experiment: [('peripheral task/bilat. stim./left target' + 'peripheral task/bilat. stim./right target') – ('peripheral task/single left target' + 'peripheral task/single right target')] – [('central task/bilat. stim.') – ('central task/left stim.' + 'central task/right stim.')]

We defined the 'competition effect' based on a significant activity increase in contrast 1 (random effects analysis, threshold: $P<0.05$, Bonferroni-corrected for the number of VOIs). We reported only on those regions that additionally showed a significant interaction effect in contrast 4 (fixed effects analysis, threshold: $P<0.05$, Bonferroni-corrected for the number of VOIs). By adding this additional positive criterion, activations that could be a pure sensory consequence of adding a distracter were eliminated. The 'invalidity effect' was defined based on an activity increase in contrast 2 (random effects analysis, threshold: $P<0.05$, Bonferroni-corrected for the number of VOIs).

If a VOI showed a significant competition effect, we also evaluated the effect of direction of attention and hemisphere using a repeated measures ANOVA with direction of attention (2 levels: valid cue/left target vs. valid cue/right target) and hemisphere (2 levels: left hemisphere vs. right hemisphere) as factors. If a VOI showed a significant invalidity effect, we also evaluated the effect of direction of shifting and hemisphere using a repeated measures ANOVA with direction of shifting (2 levels: invalid cue/left target vs. invalid cue/right target) and hemisphere (2 levels: left hemisphere vs. right hemisphere) as factors.

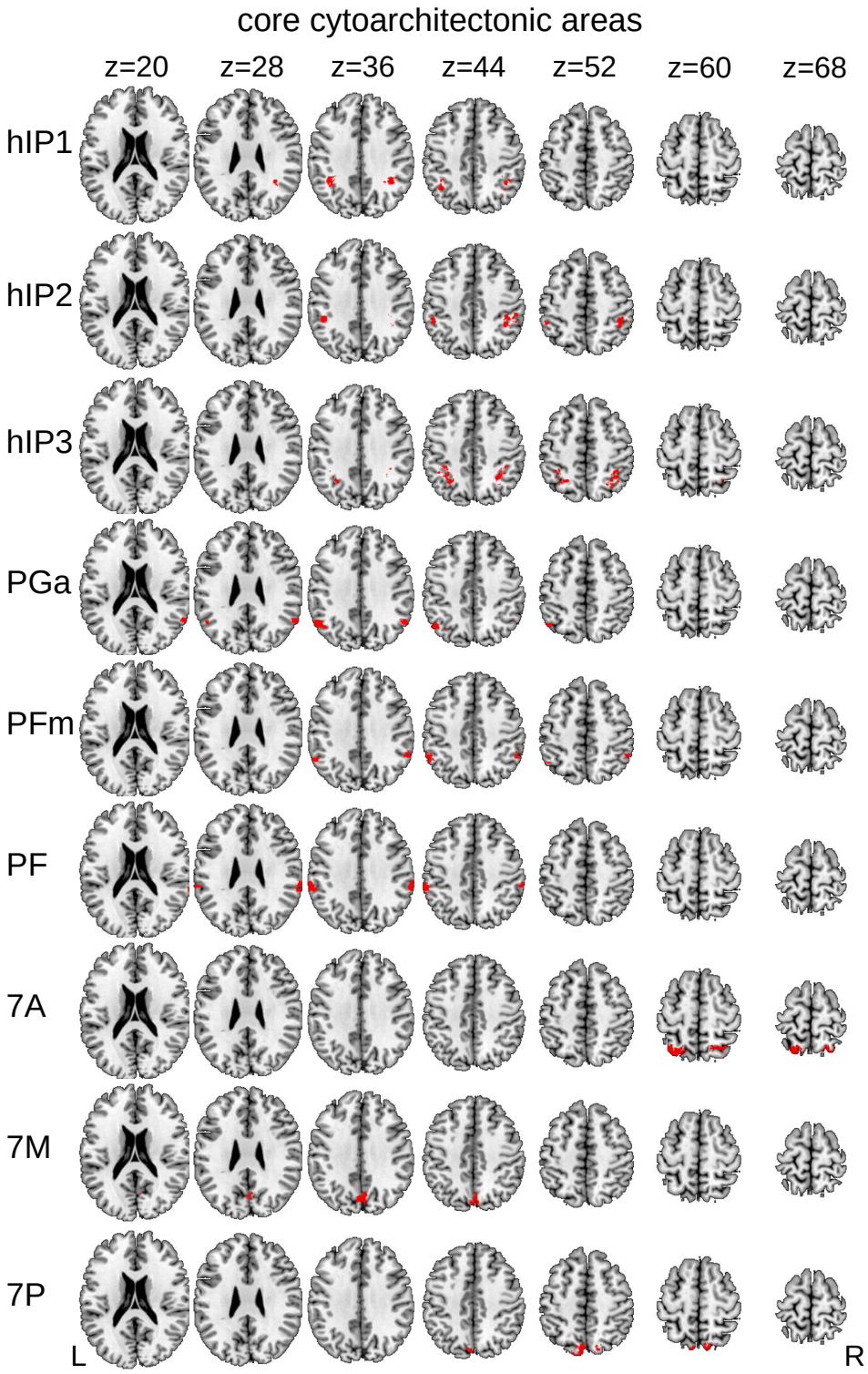

Figure 3 – **Core cytoarchitectonic areas in parietal cortex** Volumes-of-interests based on cytoarchitectonic probabilistic maps covering the intraparietal sulcus (hIP1, hIP2, hIP3), the inferior parietal cortex (PGa, PFm, PF) and the superior parietal lobule (7A, 7M, 7P), projected onto axial slices of the brain. Other VOIs that we examined are 7PC, 5Ci, 5L, 5M, PFcm, PFt and PFop. See also Table 1 for the minimum probability for inclusion of voxels within each of the VOIs and their extent.

Table 1 – **Volumes-of-interest based on cytoarchitectonic probabilistic maps** We defined 34 VOIs based on the cytoarchitectonic probabilistic maps of areas in the parietal cortex (Caspers et al., 2006; Choi et al., 2006; Scheperjans et al., 2008a,b). The minimum probability for inclusion of voxels within a given VOI (3rd and 5th column) was flexibly adapted as to reach a minimum volume of 799 mm^3 (29 voxels of 3×3×3 mm^3). The number of voxels in each VOI is given in the 2nd and 4th column.

	left hemisphere		right hemisphere	
cytoarchitectonic area	voxels (27 mm^3)	probability threshold	voxels (27 mm^3)	probability threshold
PF	59	80%	61	90%
PFcm	31	60%	61	50%
PFm	44	60%	36	90%
PFop	39	60%	68	40%
PFt	36	60%	47	60%
PGa	72	60%	46	80%
PGp	79	70%	40	90%
5Ci	30	40%	53	40%
5L	80	50%	33	70%
5M	48	50%	36	60%
7A	74	80%	42	80%
7M	30	40%	44	40%
7P	47	60%	31	80%
7PC	41	50%	43	60%
hIP1	38	50%	40	40%
hIP2	36	50%	73	30%
hIP3	64	40%	64	40%

2.6.2 Intrinsic functional connectivity

Cytoarchitectonic VOIs that showed significant effects of invalidity or competition were then subjected to a resting-state functional connectivity analysis to evaluate whether functional dissociations were reflected by connectivity differences. Intrinsic functional connectivity analysis was carried out with SPM5, supplemented by in-house software written in MATLAB (MathWorks, Natick, MA) and previously used by Ebisch et al. (2011), Gillebert et al. (2011) and Pravatà et al. (2011). The pre-processing steps for seed-based functional connectivity analysis (Fox et al., 2005; Gillebert et al., 2011) consisted of (1) band-pass filtering of the EPI scans between 0.009 and 0.08 Hertz; (2) removal by linear regression of white matter and ventricle signals, and their first derivatives; (3) removal by linear regression of three-dimensional motion parameters, and their first derivatives. After preprocessing, a representative blood-oxygenation level-dependent (BOLD) time course was obtained for each seed VOI by averaging the signals of the voxels within the seed. We then created a functional connectivity matrix by calculating cross-correlations between VOI time courses at the single-subject level. A group-level matrix was generated by converting the single-subject matrices to Z-scores by means of the Fisher's r-to-Z transformation and by subsequently applying a random effects analysis across subjects.

Prior to determining the seed-based connectivity of the parietal areas with areas at a distance, we assessed the functional connectivity within the set of parietal areas. We assessed the relative similarity of different VOI time courses by applying hierarchical cluster analysis with average linkage function (Everitt et al., 2001). We also used the resulting dendrogram to sort the functional connectivity matrix, so that VOIs with similar time courses were positioned adjacent to each other.

We also calculated whole-brain connectivity maps to assess the spatial distribution of areas functionally connected to specific cytoarchitectonic VOIs. Accordingly, we calculated for all individual participants the temporal correlation between the seed time course and the time courses of each brain voxel (Fox et al., 2005, 2006). After applying Fisher's r-to-Z transformation to each correlation map, a random effects analysis was performed to reveal group-level functional connectivity patterns (significance threshold: $P<0.001$, FDR corrected for multiple comparisons; minimum cluster extent of 30 voxels) (Fox et al., 2006).

2.7 Task-related fMRI: voxel-wise analysis

We also examined how the conventional voxel-based activation map related to the maximum probability map of cytoarchitectonic areas (MPM, Eickhoff et al., 2005, 2006), a summary map of different probabilistic cytoarchitectonic maps (Fig. 1). In the MPM, each voxel is attributed to the most likely cytoarchitectonic area at that position, resulting in non-overlapping representations of all cytoarchitectonic areas. The EPI images were spatially smoothed using a Gaussian kernel with FWHM = $5\times5\times7$ mm^3. For each subject, a contrast image was calculated for contrasts 1-4. We defined the 'competition map' based on a significant activity increase in contrast 1 (random effects analysis, threshold: voxel-level uncorrected $P<0.001$, cluster-level FWE-corrected $P<0.05$) together with a significant interaction in contrast 4 (fixed effects analysis, threshold: voxel-level uncorrected $P<0.001$, cluster-level FWE-corrected $P<0.05$). The 'invalidity map' was defined based on contrast 2 (random effects analysis, voxel-level uncorrected $P<0.001$, cluster-level FWE-corrected $P<0.05$). To evaluate any overlap between the competition and invalidity maps at a higher level of sensitivity, we also performed an analysis at a threshold of $P<0.05$, voxel-level uncorrected. The competition map and the invalidity map were directly compared to the MPM of cytoarchitectonic areas (Eickhoff et al., 2005) (Fig. 1). The degree of overlap between an activity cluster and a cytoarchitectonic MPM area was evaluated by means of two measures (Eickhoff et al., 2005):

1. the percentage of a given cytoarchitectonic MPM area that is occupied by the activity map

2. the percentage of the activity cluster that belongs to the cytoarchitectonic MPM area

We also evaluated whether the overlap was situated in the centre or at the periphery of the cytoarchitectonic area (called 'central tendency', Eickhoff et al., 2007). Since the Jülich-Düsseldorf cytoarchitectonic atlas is based on the histological examination of 10 post-mortem brains, voxels are assigned to a given cytoarchitectonic area with a 'probability class' ranging between 0% and 100% in steps of 10%. We included in each cytoarchitectonic area all voxels with a probability of 10% or higher. Next, the distribution of probabilities within this area was compared to the distribution of probabilities within the overlap between the activity cluster and the cytoarchitectonic area. For each probability class, this was mathematically expressed as the difference between the percentage of voxels in the overlap belonging to that probability class (P_{obs}, observed class representation), and the percentage of voxels in the entire cytoarchitectonic area belonging that probability class (P_{exp}, expected class representation):

$$P_{obs-exp} = \frac{P_{obs} - P_{exp}}{P_{exp}} \quad (1)$$

We also computed P_{excess}, i.e. the ratio of the cytoarchitectonic probability averaged over the voxels belonging to the overlap and the cytoarchitectonic probability averaged over all voxels belonging to a cytoarchitectonic area. A P_{excess} larger than 1 indicates a rather central location of the activation with respect to the cytoarchitectonic area, a P_{excess} smaller than 1 a more peripheral one (Eickhoff et al., 2007).

When an activity cluster in the competition or invalidity map overlapped with a cytoarchitectonic MPM area, we also determined how consistent the activation within the cytoarchitectonic MPM area was between the participants of the main experiment, i.e. in how many of the 16 subjects this voxel or one of its direct neighbours (Juch et al., 2005; Seghier et al., 2008) reached significance (threshold: uncorrected $P<0.001$).

3 Results

3.1 Behavioral performance

3.1.1 Main experiment

The orientation difference to be discriminated during the main experiment was 8.6°, averaged across subjects and runs (range 6-11°).

The main effect of trial type (valid cue/single target, invalid cue, bilat. stim.) was significant for d' ($F_{2,30}$=8.01, P=0.002) and for RTs ($F_{1.22,18.32}$=32.08, $P<0.0001$). Subjects were significantly less accurate and slower for invalidly cued trials (d': P=0.0009; RTs: $P<0.0001$) and bilateral stimulation trials (d': P=0.004; RTs: $P<0.0001$) compared to valid cue/single target trials. Performance did not differ between invalidly cued trials and bilateral stimulation trials (d': P=0.47; RTs: P=0.07) (Table 2A). There was no main effect of target location (d': $F_{1,15}$=0.24, P=0.63; RTs: $F_{1,15}$=0.52, P=0.48) and no interaction effect (d': $F_{2,30}$=0.07, P=0.93; RTs: $F_{1.18,17.77}$=1.00, P=0.35).

The number of saccades into the left or right visual field did not differ between conditions according to a two-way repeated measures ANOVA with task condition and target location as factors (main effect of task condition: $F_{1.12,16.87}$=1.68, P=0.56; main effect of target location: $F_{1,15}$=4.16, P=0.06; interaction between task condition and target location: $F_{2,30}$=0.29, P=0.75). Overall the number of saccades per condition per run was low (mean±standard error of the mean: 1.23±0.27).

Table 2 – **Behavioral parameters** Mean ± standard error

condition	% correct	d'	reaction time
A. Main experiment			
valid cue / single left target	89±1	2.75±0.12	714±24
valid cue / single right target	89±1	2.79±0.14	709±27
invalid cue / left target	84±1	2.38±0.17	778±26
invalid cue / right target	86±1	2.49±0.14	792±30
bilat. stim. / left target	84±2	2.30±0.15	804±30
bilat. stim. / right target	85±2	2.39±0.17	819±43
B. Sensory control experiment			
peripheral task / single stim.	90±2	2.80±0.18	657±9
peripheral task / bilat. stim.	85±2	2.10±0.16	760±21
central task / single stim.	81±2	2.05±0.22	680±15
central task / bilat. stim.	82±3	1.88±0.16	690±18

3.1.2 Sensory control experiment

There was a significant main effect of task on d' (d': $F_{1,23}$=9.81, P=0.005; RTs: $F_{1,23}$=1.48, P=0.24): subjects were less accurate during the central than during the peripheral attention task (Table 2B). There was a significant main effect of stimulus display (single versus bilateral stimulation) on performance (d': $F_{1,23}$=9.12, P=0.006; RTs: $F_{1,23}$=28.53, P<0.0001), and a significant interaction between task and stimulus display (d': $F_{1,23}$=4.72, P=0.04; RTs: $F_{1,23}$=19.56, P=0.0002) (Table 2B). For the peripheral task, subjects were significantly less accurate and slower during bilateral stimulation trials than during single grating trials (d': P=0.003; RTs: P<0.0001). This was not the case for the central attention task (d': P=0.32; RTs: P=0.42) (Table 2B).

The number of saccades into the left or right visual field did not differ between conditions according to a repeated measures ANOVA (main effect of task: $F_{1,23}$=0.31, P=0.58; main effect of stimulus display: $F_{1,23}$=2.17, P=0.15; interaction between task and stimulus display: $F_{1,23}$=1.93, P=0.18) (average number of saccades per condition per run: 2.86±0.48).

3.2 Volume-of-interest analysis of task-related fMRI data

3.2.1 Competition effect

Areas hIP1, hIP3 and PFm bilaterally fulfilled our criterion for a competition effect: when subjects attended to a peripheral grating and an irrelevant contralateral distracter was added, activity was significantly increased compared to the single target condition (contrast 1) (Fig. 4A, Suppl. Table 1). This activity increase was not seen during central attention conditions (significant interaction according to contrast 4) (Fig. 4B, Suppl. Table 2). In hIP3, activity was also significantly higher during bilateral stimulation than during invalidly cued trials (contrast 3) (left hIP3: P=0.005; right hIP3: P=0.004) (Figs. 4A, 5A). A similar trend was observed in hIP1 (left hIP1: P=0.03; right hIP1: P=0.03) (Figs. 4A, 5A). Conversely, in area PFm the invalidity and the competition effect were both significant and of similar effect size (contrast 3: P>0.82) (Figs. 4A, 5C). The effect of direction of attention remained below the significance level (P>0.06). Neither was there any interaction between the direction of attention and hemisphere (P>0.12).

3.2.2 Invalidity effect

Areas PGa, PFm, right PF and left 7M showed a significant invalidity effect (contrast 2) (Fig. 4A, Suppl. Table 1). Activity in area PF to the right was significantly higher during invalid

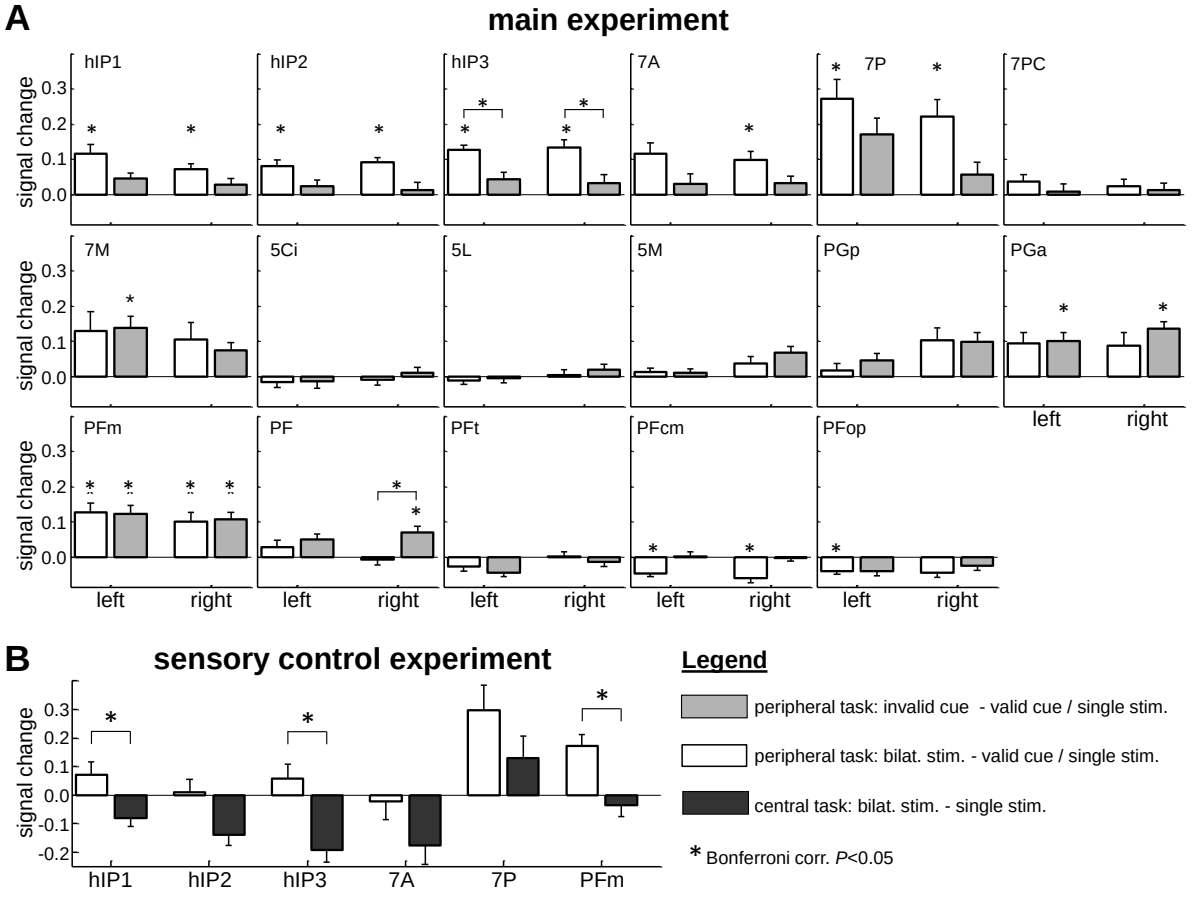

Figure 4 – Volume-of-interest analysis: cytoarchitectonic mapping of attentional selection and reorienting (**A**) Main experiment: Relative effect size of contrast 1 (in white) and contrast 2 (in light grey) in each VOI defined based on cytoarchitectonic probabilistic maps in the intraparietal sulcus (hIP1, hIP2, hIP3), superior parietal lobe (7A, 7P, 7M, 7PC, 5L, 5M, 5Ci), angular gyrus (PGp, PGa) and supramarginal gyrus (PFm, PF, PFt, PFcm, PFop). Mean and standard error across subjects are shown (N=16, random effects analysis). Significant effects are indicated with an asterix (threshold: $P<0.05$, Bonferroni-corrected for the number of VOIs). (**B**) Sensory control experiment: Relative effect size of the interaction effect between task and stimulus display (contrast 4) in each VOI that showed a significant activity increase for valid/bilat. stim. relative to valid/single stim. trials (contrast 1) in the main experiment: hIP1, hIP2, hIP3, 7A, 7P and PFm. Mean and standard error across runs are shown (N=24, fixed effects analysis). Significant effects are indicated with an asterix (threshold: $P<0.05$, Bonferroni-corrected for the number of VOIs).

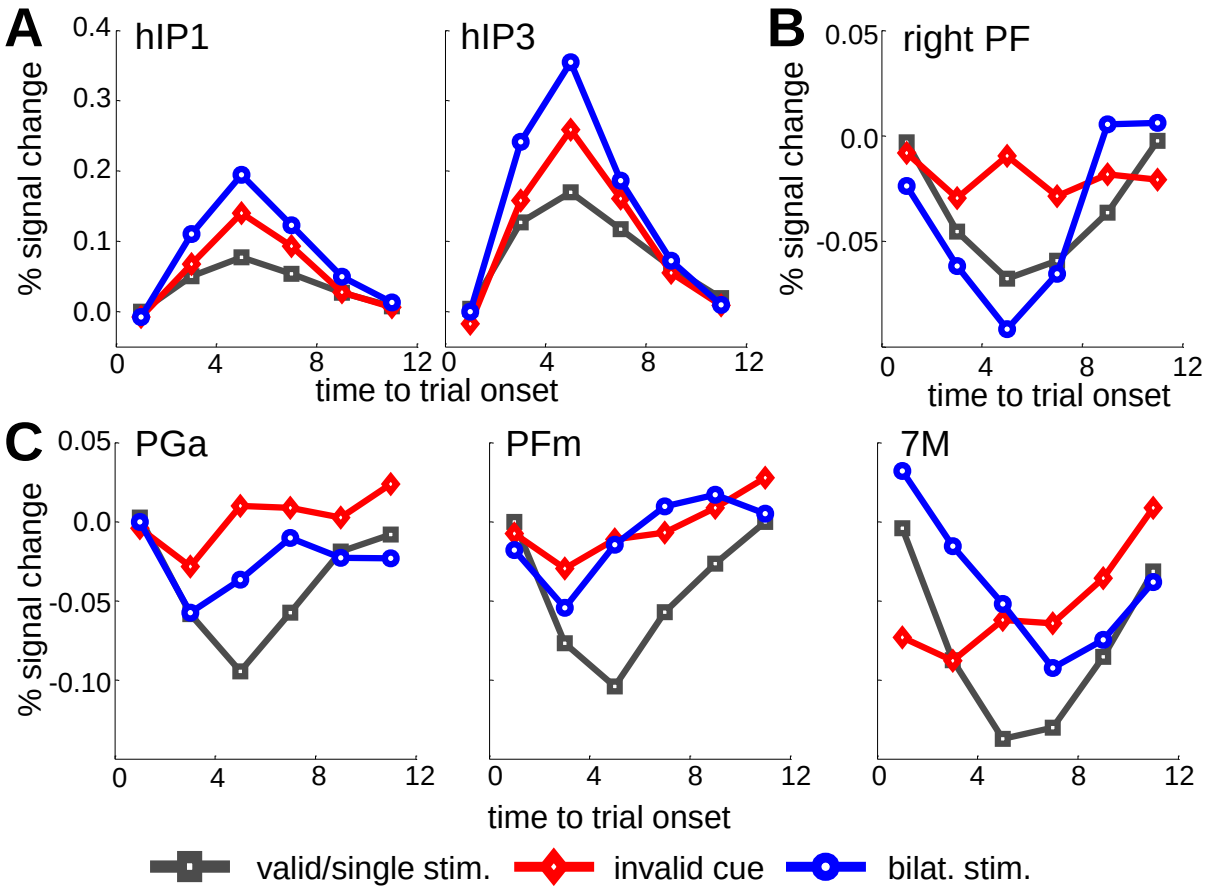

Figure 5 – **Volume-of-interest analysis: cytoarchitectonic areas showing a competition or invalidity effect** Main fMRI experiment: time-activity curves averaged over all 16 subjects and all voxels belonging to the VOIs defined based on cytoarchitectonic probabilistic maps in (**A**) hIP1 and hIP3, (**B**) right PF, and (**C**) PGa, PFm and 7M. Since no interhemispheric differences in % signal change were observed in hIP1, hIP3, PGa, PFm and 7M, data were pooled across hemispheres.

cue/single target than during bilateral stimulation trials (contrast 3: P=0.0004) (Figs. 4A, 5B). No significant difference was observed between the competition and the invalidity effect in PGa, PFm or left 7M (P>0.14) (Figs. 4A, 5C). Activity in these areas did not depend on the direction of shifting (P>0.24). Neither was there any interaction between the direction of shifting and hemisphere (P>0.41).

3.3 Intrinsic functional connectivity

We compared the resting-state fMRI activity in these cytoarchitectonic VOIs to assess their connectional properties. First, we calculated a correlation matrix between areal time courses, which was then sorted on the basis of a hierarchical cluster analysis (Fig. 6A-B). Activity in identical cytoarchitectonic areas was correlated between hemispheres. Furthermore, we observed that the time courses of areas in the intraparietal sulcus (hIP1, hIP3) and PFm were highly correlated. Finally, the right PF in the inferior parietal cortex had the most specific temporal profile compared to other areas (Fig. 6A): its time course was not significantly correlated with the time course of any of the other parietal areas (Fig. 6B).

To assess the long-range connectional properties of these cytoarchitectonic VOIs, we calculated whole-brain functional connectivity maps. We focused on areas in the right parietal cortex, and in particular hIP1, PFm, PGa and PF, as hierarchical clustering showed these areas to have relatively distinct temporal profiles (Fig. 6A). On a general level, the functional con-

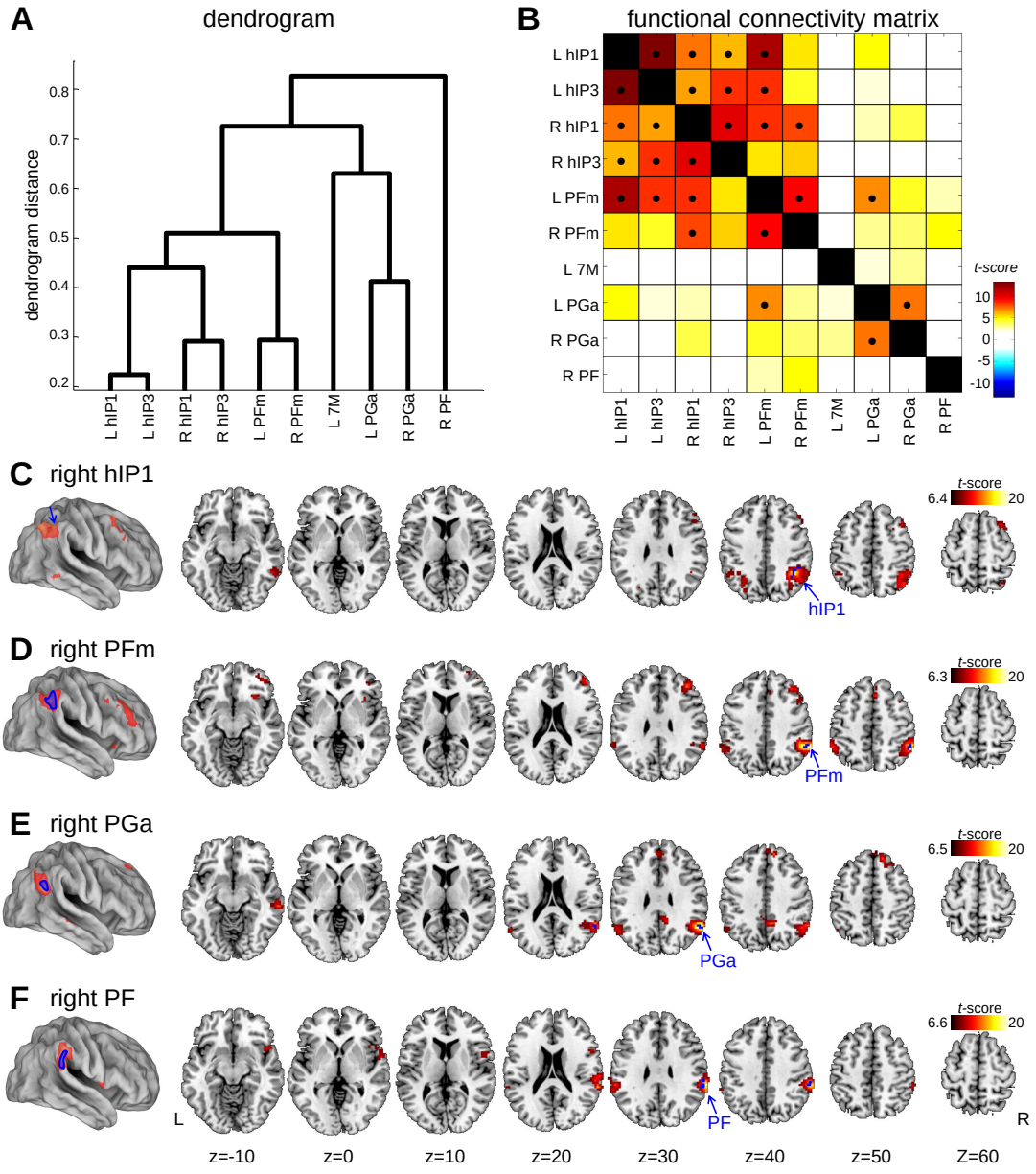

Figure 6 – **Resting-state functional connectivity analysis** Resting-state functional connectivity analysis from cytoarchitectonic areas that showed a significant competition or invalidity effect in the volume-of-interest analysis (Fig. 4A). Spontaneous activity was extracted from resting-state fMRI data by averaging the time courses across voxels in specific seed regions (see Fig. 3 and Table 1). (**A**) Hierarchical clustering is performed using the cross-correlations between the time courses as similarity metric. (**B**) The cross-correlation matrix is sorted on the basis of the hierarchical clustering results, so that adjacent VOIs have the most similar connectivity profiles. Significant correlations ($P<0.05$, Bonferroni-corrected for the number of pairwise comparisons) are indicated by a black dot. (**C-F**) Group-level functional connectivity maps from areas (**C**) right hIP1, (**D**) right PFm, (**E**) right PGa, (**F**) right PF are shown on axial slices of the brain, along with the seed region (indicated in blue). These group-level maps (t-maps) result from a random effects analysis of single-subject correlation maps (expressed in Z-scores). The colored areas in each map represent the cortical regions that are significantly connected to the seed (threshold: voxel-level FDR-corrected $P<0.001$).

Table 3 – Voxel-wise analysis of attentional selection and reorienting Stereotactic MNI (Montreal Neurological Institute) coordinates of brain areas showing (**A**) a significant competition effect (contrast 1 and contrast 4), and (**B**) a significant invalidity effect (contrast 2). Threshold: voxel-level uncorrected $P<0.001$, cluster-level FWE-corrected $P<0.05$. Extent, $3\times3\times3$ mm^3 voxels.

Region	x	y	z	Z	extent	P
	(MNI)			(peak)	(voxels)	(FWE-corr)
A. Competition effect (contrast 1 ⋂ contrast 4)						
right IPS	42	-42	48	5.62	219	<0.001
left IPS	-33	-57	48	5.09	207	<0.001
right SPL	9	-66	51	5.00	57	<0.001
left precentral gyrus	-48	3	39	4.69	42	<0.001
B. Invalidity effect (contrast 2)						
left inferior/middle frontal gyrus	-39	15	33	5.67	453	<0.001
left middle temporal gyrus	-63	-54	0	5.41	148	<0.001
right IPL	57	-45	18	4.83	481	<0.001
right inferior frontal gyrus	39	0	39	4.73	210	<0.001
left IPS	-48	-48	33	4.59	267	<0.001
medial SPL	3	-63	51	4.48	209	<0.001

nectivity maps revealed that the four selected areas belonged to distinct resting-state networks. The functional connectivity map from right hIP1 largely included the middle temporal complex, the frontal eye fields and a portion of the adjacent middle frontal cortex (Fig. 6C). These areas belong to what has been called the dorsal attention network (Corbetta and Shulman, 2002). Seeding in right PFm yielded the dorsolateral (including the middle frontal gyrus and inferior frontal sulcus) and rostral prefrontal cortex, the anterior insula, and the dorsomedial prefrontal cortex (Fig. 6D). This network is spatially consistent with the multiple-demand (Duncan, 2010) or executive control network (Seeley et al., 2007), but also overlaps in part with the dorsal attention network (Fig. 6C). Seeding in right PGa yielded a different map, including the angular gyrus, posterior cingulate and rostral prefrontal cortex (Fig. 6E), corresponding to the default mode network (Buckner et al., 2008; Greicius et al., 2003). Finally, the functional connectivity map from right PF included the inferior frontal gyrus and insula (Fig. 6F), areas belonging to the ventral attention network (Corbetta and Shulman, 2002).

3.4 Whole-brain voxel-wise analysis of task-related fMRI

3.4.1 Competition effect

The spatial map corresponding to the competition effect (contrast 1 combined with contrast 4, Table 3A) included clusters in the left and right IPS that overlapped mainly with cytoarchitectonic areas hIP1-3 (Fig. 7A, blue outline; Table 4A). The activity clusters were located towards the centre of areas hIP1-3 ($P_{excess} > 1$) (Fig. 8A-B). The ratio between the cytoarchitectonic probabilities observed in the area of overlap, and the cytoarchitectonic probabilities in the whole cytoarchitectonic area was highest for hIP3 ($P_{excess} > 1.45$) (Fig. 8A-B). Inter-subject consistency of the competition effect was also higher in hIP3 compared to the other areas (Table 4A).

We also identified a cluster in the medial wall of right SPL, overlapping with right 7A and 7P (Fig. 7A, blue outline; Table 4A). Inter-subject consistency of the competition effect (Table 4A) and P_{excess} (Fig. 8C) were higher for 7A than for 7P.

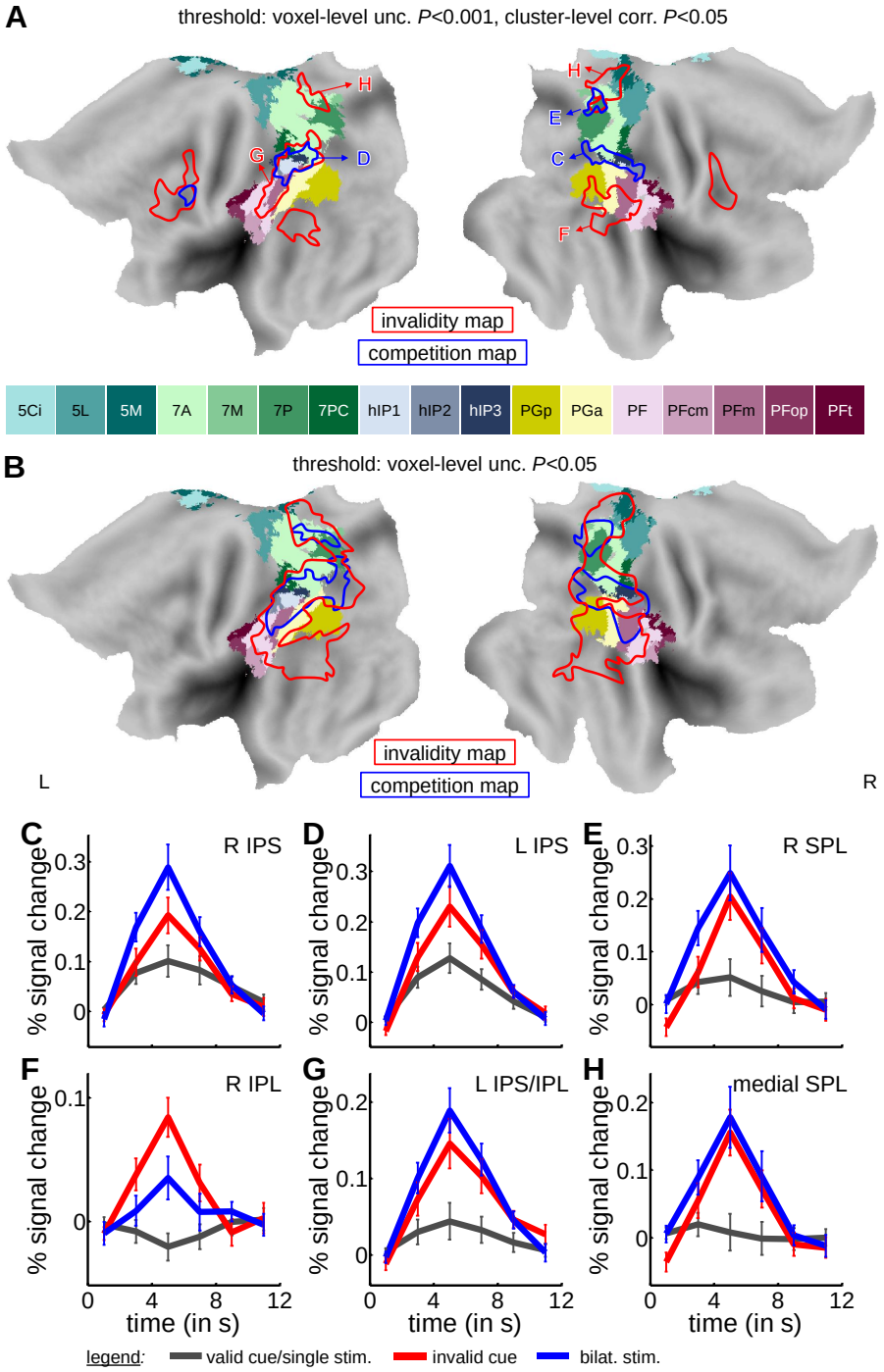

Figure 7 – **Voxel-wise analysis of attentional selection and reorienting** (**A-B**) The maximum probability (MPM), the competition map (contrasts 1 and 4, blue outline) and the invalidity map (contrast 2, red outline) are projected onto a surface rendering of the brain (flattened view) (Van Essen, 2005). (**A**) Threshold: voxel-level uncorrected $P<0.001$, cluster-level FWE-corrected $P<0.05$. (**B**) Threshold: voxel-level uncorrected $P<0.05$. Only parietal activity clusters are shown. (**C-E**) Competition effect: time-activity curves averaged over all 16 subjects and all significant voxels in (**C**) right IPS, (**D**) left IPS and (**E**) right SPL, defined based on contrasts 1 and 4 (threshold: voxel-level uncorrected $P<0.001$, cluster-level FWE corrected $P<0.05$). (**F-H**) Invalidity effect: time-activity curves averaged over all 16 subjects and all significant voxels in (**F**) right IPL, (**G**) left IPS/IPL and (**H**) medial SPL, defined based on contrast 2 (threshold: voxel-level uncorrected $P<0.001$, cluster-level FWE corrected $P<0.05$).

Table 4 – Probabilistic volume-based MPM labelling of parietal cortex activations during attentional selection and reorienting Brain areas in parietal cortex that showed (**A**) a significant competition effect (contrast 1 and contrast 4) and (**B**) a significant invalidity effect (contrast 2). See also Table 3. Threshold: voxel-level uncorrected $P<0.001$, cluster-level FWE-corrected $P<0.05$. The maximum probability map of cytoarchitectonic areas was used to interpret the locations of the cluster within subdivisions of IPS, SPL and the inferior parietal cortex. For each significant cluster, the probabilistic cytoarchitectonic area (column 2), percentage of activation in the area (column 3), percentage of cluster in the area (column 4) and the percentage overlap across subjects in that area (threshold: uncorrected $P<0.001$) (column 5) are given. Only cytoarchitectonic areas overlapping with more than 5% of the cluster are reported.

cluster	volume-based MPM-labelling				% overlap across subjects
	overlap with area		% area activated	% cluster in area	
A. Competition effect (contrast 1 ⋂ contrast 4)					
right IPS	right	hIP3	75	30	61
	right	7A	7	10	42
	right	hIP2	48	9	49
	right	hIP1	24	8	37
left IPS	left	hIP1	51	35	59
	left	hIP3	60	23	62
	left	hIP2	34	12	48
	left	7A	3	7	46
	left	PFm	7	5	38
right SPL	right	7A	6	37	42
	right	7P	7	26	39
B. Invalidity effect (contrast 2)					
right IPL	right	PFm	38	20	34
	right	PGa	32	20	38
	right	PGp	10	7	22
	right	PF	9	5	14
left IPL	left	PF	19	21	23
	left	PFm	33	19	30
	left	hIP1	33	17	28
	left	hIP3	30	9	23
	left	7A	5	9	33
	left	hIP2	33	9	23
	left	PGa	7	6	18
medial SPL	left	7A	7	16	33
	right	7A	9	16	36
	left	7P	14	11	19
	right	5M	11	7	17

3.4.2 Invalidity effect

The spatial map corresponding to the invalidity effect (contrast 2, Table 3B) included a cluster in the right inferior parietal lobule (Fig. 7A, red outline), encompassing mainly cytoarchitectonic areas PGa and PFm (Table 4B), extending into the superior temporal gyrus (Fig. 7A). The inter-subject consistency of the invalidity effect (Table 4B) was highest in PGa and PFm. The overlap between this activity cluster and the MPM area of right PF was relatively low (5% of the cluster, 9% of right PF activated). Right PF, however, was the only area in the inferior parietal cortex overlapping with the invalidity map and not with the competition map, even when lowering the threshold for both maps to an uncorrected $P<0.05$ (Fig. 7B).

A second cluster in the invalidity map encompassed the left inferior parietal lobule and extended into IPS (Fig. 7A). This cluster mainly overlapped with cytoarchitectonic MPM areas hIP1-3, PF and PFm (Table 4B). P_{excess} indicated a central location of the cluster with respect to hIP1-3 and PFm (Fig. 8E).

We observed a third cluster in the medial wall of SPL overlapping with left 7A-7P and right 7A-5M (Table 4B), with P_{excess} being highest for areas 7A-7P (>1) (Fig. 8F).

4 Discussion

We directly related fMRI activity patterns during spatial reorienting and attentional selection to the probabilistic cytoarchitectonic map of parietal cortex (Caspers et al., 2006, 2008; Choi et al., 2006; Scheperjans et al., 2008a,b). Starting from cytoarchitectonic volumes-of-interest we characterized the volumes functionally, and, inversely, starting from the fMRI activity clusters we determined the most likely cytoarchitectonic labelling. At least 3 cytoarchitectonic areas within right inferior parietal cortex showed a significant invalidity effect: PGa, PFm, and PF (Figs. 4, 7A-B, Table 4B). As the only area, right PF showed a relatively exclusive response to invalidly cued trials (Figs. 4, 5B). hIP1 and hIP3 were the only parietal areas where the competition effect was significantly stronger than the invalidity effect (Figs. 4, 5A). PFm and PGa showed both an invalidity and a competition effect (Figs. 4, 5C) .

We defined the competition effect based on a dual criterion: a significant increase during the competition trials in the main experiment as well as a significant interaction between task and stimulus display in the sensory control experiment. The latter positive criterion allowed us to eliminate those regions where activation could be a pure sensory consequence of adding a distracter. We did not combine the criteria in a formal mathematical procedure (such as a conjunction) given the difference in sample size between the main experiment and the sensory control experiment. The control experiment was based on only four subjects and may therefore have missed some areas where an interaction was present below the detection threshold. The significant interaction effect we observed in middle IPS was in full agreement with a series of previous experiments (Gillebert et al., 2012a; Molenberghs et al., 2008; Vandenberghe et al., 2005). These experiments have shown in larger samples of subjects (up to 22) a significant interaction between task (central versus peripheral attention) and stimulus display (single versus double stimulation) in the same regions as those obtained by the current fixed effects analysis. The high between-study consistency of this interaction effect in the middle IPS segment indicates robustness of this finding.

Our task-related fMRI data revealed that at least 3 of the cytoarchitectonic areas in the inferior parietal cortex, namely PFm, PGa and PF, show a significant invalidity effect (Figs. 4, 7A). The overlap between the invalidity map and the cytoarchitectonic MPM areas in the right inferior parietal cortex was largest in PFm and PGa (Table 4B). However, the activity increase in these areas was not limited to invalidly cued trials. When subjects oriented their attention to a peripheral target and a distracter was added to the display, these areas also showed an activity increase (Figs. 4, 5C). Among all cytoarchitectonic areas showing an invalidity effect,

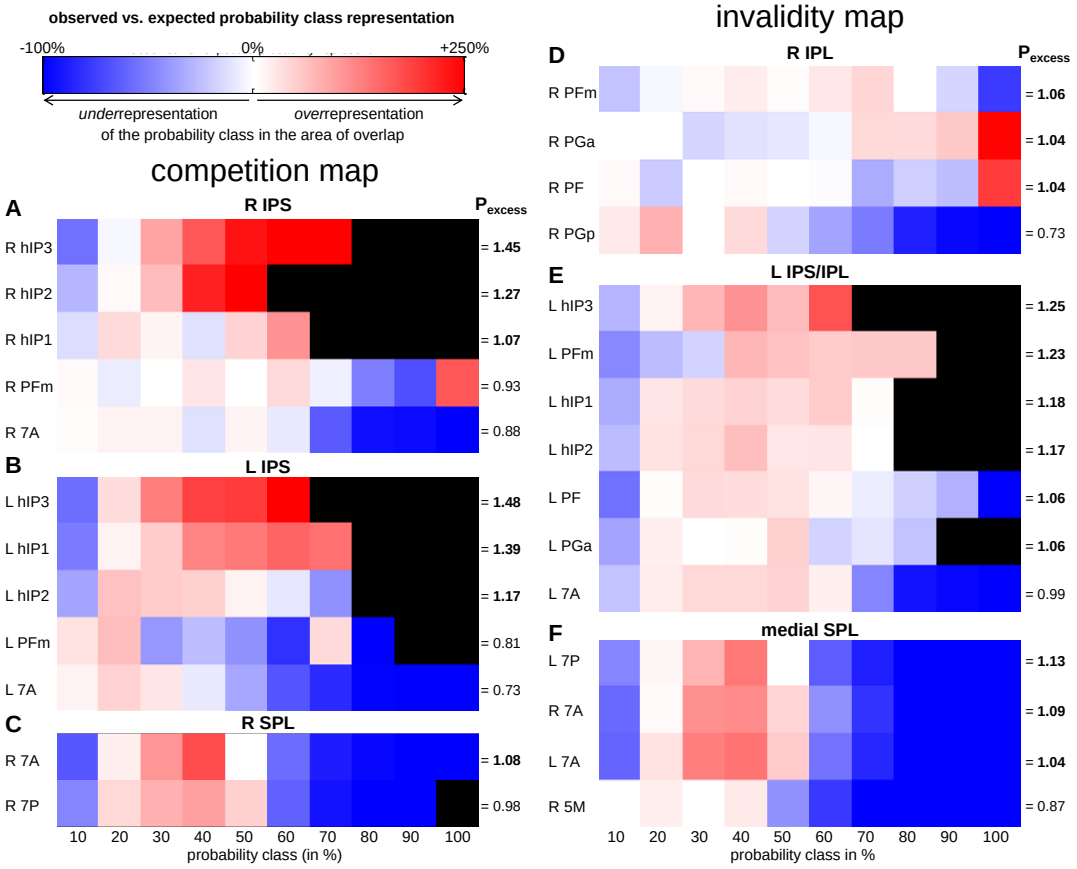

Figure 8 – Comparison of frequency of probability classes in the overlap vs. the entire cytoarchitectonic map (**A-C**) Distribution-based analysis of the competition map: cytoarchitectonic areas that overlapped with the competition map (contrast 1 inclusively masked by contrast 4, threshold: voxel-level uncorrected $P<0.001$, cluster-level FWE-corrected $P<0.05$) are displayed in rows, different probability classes (10%-100%) are displayed in columns. The relative *under*representation of a probability class in the area of overlap is colour coded from dark blue (-100%, indicating a probability class not found in the cluster) to white (0%, indicating a similar distribution in the area of overlap and the entire cytoarchitectonic map) on a continuous scale. The relative *over*representation of a probability class is coded from white (0%) to red (250%, indicating maximum overrepresentation, Equation 1). Black boxes indicate probability classes that were not present in the respective cytoarchitectonic area according to Caspers et al. (2006); Choi et al. (2006); Caspers et al. (2008); Scheperjans et al. (2008a,b). The value P_{excess} is given to the right of the table. See main text for definition and interpretation of this value. (**D-F**) Distribution-based analysis of the invalidity map (contrast 2, threshold: voxel-level uncorrected $P<0.001$, cluster-level FWE-corrected $P<0.05$). **Example panel A:** The R IPS activation consisted of 219 voxels, of which 182 overlapped with the un-threshold probabilistic map of right hIP3. Out of those 182 voxels, 32 corresponded to locations where hIP3 was found with 40% probability. The relative frequency of '40% voxels' for hIP3 in the cluster was thus 17.6% (32/182). However, amongst the entire probabilistic map for hIP3, the relative frequency of '40%' voxels was only 6.5%. Therefore, the 40% probability class was *over*represented by +170% [(17.6-6.5)/6.5]. In contrast, the 10% probability class was *under*represented by -56% (22.6% in the activated hIP3 voxels vs. 51.3% of all hIP3 voxels).

only right PF was specifically involved in attentional reorienting. This was demonstrated both by a volume-of-interest analysis (Fig. 4A) and by a voxel-wise analysis of task-related fMRI data (Fig. 7A-B). The fraction of the invalidity map that overlapped with right PF was relatively small and only a relatively restricted portion of right PF showed an invalidity effect (Fig. 7A, Table 4B). This response of PF to invalidly cued trials cannot be attributed to a breach of expectancy or to the low frequency of invalidly cued trials (Arrington et al., 2000; Corbetta et al., 2000; Downar et al., 2000; Vossel et al., 2006): the expectancy rate of invalidly cued and bilateral stimulation trials was matched (Fig. 2B) and only invalidly cued trials yielded an activity increase compared to validly cued, single target trials. Bilateral stimulation trials, as well as validly cued, single target trials, yielded similar activity decreases compared to baseline (Figs. 4, 5B). Such an exclusive activation during invalidly cued as opposed to competition trials fits with the hypothesis that right PF is specifically recruited when subjects reorient towards stimuli that stand out against the background by being perceptually or emotionally salient (Corbetta et al., 2008; Gillebert et al., 2012b; Nardo et al., 2011; Vandenberghe et al., 2012).

Prior to evaluating the functional connectivity with more remote areas, we applied hierarchical clustering analysis to determine the connectivity structure within the set of parietal areas studied. From this analysis, we observed that right PF stood apart from all other parietal areas studied, that the time course in hIP1/3 correlated relatively well with that of PFm, and, thirdly, that homotopical left and right-sided areas showed similar time courses (Fig. 6A-B). With regard to seed-based functional connectivity with more remote areas, we followed a whole-brain mapping strategy similar to that used by Uddin et al. (2010). Seed-based connectivity mapping of resting-state fMRI data constitute a powerful means to probe the parcellation of the parietal cortex (Cohen et al., 2008), as it provides task-independent measures that reflect underlying anatomical connectivity (Skudlarski et al., 2008). The delineation of functional connectivity maps is dependent on the exact definition of the seed used. In our study, we have used the 'core' of cytoarchitectonic areas to define replicable seeds on the basis of strict anatomical criteria (Fig. 3, Table 1). Right PF was mainly connected with inferior frontal gyrus and anterior insula (Fig. 6F), constituting what has been called the ventral attention network (Corbetta and Shulman, 2002). PFm and PGa, which shared a very similar task-related fMRI response (Figs. 4, 5C), could be further subdivided based on their pattern of connectivity with the rest of the brain. PGa was linked with the default mode network (Fig. 6E), in accordance with previous suggestions based on cytoarchitectonic mapping (Wu et al., 2009) and with diffusion tensor imaging (DTI) tractography (Uddin et al., 2010). In contrast, PFm was mainly connected with the middle frontal gyrus and dorsomedial prefrontal cortex (Fig. 6D), corresponding to a network that has been called 'multiple demand network' (Duncan, 2010) or 'executive control network' (Seeley et al., 2007). Areas hIP1 and hIP3 showed marked functional connectivity with frontal areas (Fig. 6C) largely belonging to the dorsal attention network (Corbetta and Shulman, 2002), but also in part to the executive control network (Seeley et al., 2007). This result may suggest that hIP1/3 and PFm, being spatially adjacent, are connected to frontal areas partially through common fiber bundles. This hypothesis would be consistent with the results of some resting-state studies that delineated brain networks in a data-driven manner without any seeding (Beckmann et al., 2005; Mantini et al., 2007).

While the IPS activations mainly resulted from increases compared to baseline (Fig. 5A), several of the inferior parietal activations resulted from differential decreases compared to baseline (Fig. 5C) (Hayes and Huxtable, 2012; Mantini and Vanduffel, 2012). The differential decrease in PGa fits with it being part of the default mode network, a set of nodes that generally show higher activity during baseline than during active conditions (Fig. 5C, 6E). Differential activity decreases were not restricted to PGa but also occurred in more anteriorly located inferior parietal areas such as PFm and PF. In epoch-based or blocked-mode experiments, decreases during the active task compared to baseline have been related to spontaneous cognitive processes occurring during baseline ('the free-wheeling mind' during 'the resting state') (Binder, 2012; Mantini

and Vanduffel, 2012). For activity decreases in fast event-related experiments, this explanation is unlikely given the rapid succession of trials and therefore the high demands in terms of processing speed to keep pace with the rapid presentation rate. Alternatively, decreases may reflect event-related suppression of activity in regions that are not involved in the task at hand (Lachaux et al., 2008) and the reallocation of resources to other regions (McKiernan et al., 2003; Slotnick et al., 2003). Such an explanation would implicate that resources are drawn away from inferior parietal areas such as PGm or PF during peripheral attention tasks. This hypothesis however goes against current evidence about the role of these areas (Corbetta and Shulman, 2011) and can therefore be dismissed. According to a third hypothesis, decreases in TPJ may relate to filtering out distracting stimuli (Shulman et al., 2007). This however cannot explain the activity pattern we observed in our study in PFm as activity during the competition trials was higher or equal to that observed during the valid cue/single stim. trials, i.e. opposite to what the filtering hypothesis would predict. To summarize, the biological significance of decreases compared to baseline in rapid event-related fMRI studies outside retinotopically organized cortex (Slotnick et al., 2003) remains to be clarified. Our main findings, however, are based on direct comparison between different event types rather than comparisons to baseline.

In contrast to right PF, hIP1/3 bilaterally showed an activity increase when a target was presented simultaneously with a competing distracter (Molenberghs et al., 2008; Vandenberghe et al., 2005). It has been suggested that hIP3 corresponds to what others called VIPS (Orban et al., 2006). Activity in this area did not vary with the direction of attention. The activity profile in the middle segment of IPS differs in this regard from that in the posterior IPS segment (Molenberghs et al., 2008; Vandenberghe et al., 2005; Vandenberghe and Gillebert, 2009; Vandenberghe et al., 2012). In posterior IPS, activity levels vary with the direction of attention (Bressler and Silver, 2010; Silver and Kastner, 2009; Vandenberghe et al., 2005; Vandenberghe and Gillebert, 2009; Yantis et al., 2002). Posterior IPS, also called IPS0 or IPS1, contains retinotopic representations of left and right visual field (Silver et al., 2005; Silver and Kastner, 2009; Swisher et al., 2007; Wandell et al., 2007). It has not been characterized yet in terms of cytoarchitecture. Areas hIP1 and hIP3 can also be functionally dissociated from the medial wall of SPL, a region which has been implicated in spatial shifting (Kelley et al., 2008; Molenberghs et al., 2007; Vandenberghe et al., 2001; Yantis et al., 2002). The medial wall of SPL was activated both for invalid and for competition trials (Fig. 7A,E,H) and partially overlapped with the medial portion of areas 7A and 7P (Fig. 7A, Table 4A-B). Its activity profile can be accounted for by a role in spatial displacement of attentional weights, which is needed for both types of trials (Molenberghs et al., 2007; Vandenberghe et al., 2001, 2012).

We localised the processes of attentional selection and reorienting using a probabilistic cytoarchitectonic reference frame. A similar approach has been adopted to elucidate the differential contribution of parietal areas to mathematical processing (Rosenberg-Lee et al., 2011; Wu et al., 2009). In these studies, the principal effects occurred in PGa and PGp, mainly consisting of differential deactivations, and in hIP1-3, mainly consisting of activations (Wu et al., 2009). Areas belonging to the supramarginal gyrus (PFm, PF, PFop or PFt) were only minimally involved during mental arithmetics. Compared to task-related fMRI, cytoarchitectonic maps offer the advantage of being independent of any specific tasks or seeds used and are therefore optimally suited for exchange of localisation data between centres. This said, cytoarchitectonic maps also have their limitations: The variability between subjects in size and borders can be relatively high in specific areas, as we have seen in hIP1-3 (Scheperjans et al., 2008a) (see also Table 1). The total sample size of brains on which the cytoarchitectonic maps are based is relatively restricted (n = 10). Furthermore, the algorithm to transform the cytoarchitectonic map into a common anatomical template (such as MNI) is most often partly based on macroanatomical landmarks, while the relationship between the cytoarchitectonic areas and these landmarks varies between subjects.

A classical tenet in visual neurophysiology is the close correspondence between cytoarchi-

tectonic demarcations, connections and functional segregation (Orban and Vanduffel, 2007). In inferior parietal cortex, however, our method yielded numerous mismatches between borders of fMRI activity foci and cytoarchitectonic boundaries: activity foci occupied only part of the cytoarchitectonic areas or overlapped with multiple adjacent areas (Fig. 7). A first explanation that comes to mind is methodological: the processes isolated by our fMRI contrasts may not fit with the true division of function laid out in the cytoarchitectonic patterns. Technically, normalisation and inter-subject variability of cytoarchitectonic areas and the spatial resolution of fMRI may prevent us from seeing the true relationship between cytoarchitectonics and functional activation as it would occur in the individual brains. More fundamentally, the lack of concordance between the borders of the functional activations and cytoarchitectonic boundaries may reflect a principle of how higher-order multimodal association cortex is organized. This raises intriguing questions about the relationship between cytoarchitectonic boundaries and functional divisions in higher-order multimodal association cortex. For instance, the neuronal circuits may integrate neuronal activity across cytoarchitectonic boundaries in a parallel and distributed manner more so than is the case in cytoarchitectonically defined upstream visual areas. While the relationship between the activity foci and the cytoarchitectonic borders was fuzzy (Fig. 7), the functional distinctions between the cytoarchitectonically defined volumes of interest were convincing, in particular the dissociation between area PF and hIP1/3.

Alternative approaches for parcellating parietal cortex are possible by means of in vivo imaging in humans, e.g. using DTI to delineate regions based structural connections. At present, DTI does not permit to distinguish efferent and afferent connections, as it can be done by neuroanatomical tracing in non-human primates (Felleman and Van Essen, 1991). In humans, DTI-based parcellation of parietal cortex seeded with superior colliculus, ventral premotor cortex and parahippocampal cortex allowed Rushworth et al. (2006) to distinguish between the middle IPS, the angular gyrus and the supramarginal gyrus, respectively, and to draw parallels with monkey areas on that basis. In particular, the angular gyrus (PGp/PGa) was shown to be strongly connected with medial temporal cortex through the inferior longitudinal fascicle. The supramarginal gyrus was connected with ventral premotor cortex through the third portion of the superior longitudinal fascicle (Rushworth et al., 2006). More recently, Mars et al. further distinguished by means of DTI three inferior parietal clusters, a dorsal and two ventral regions (Mars et al., 2011, 2012). The 3 regions had their center of gravity in areas PFm, PGa and PF, respectively (Eickhoff et al., 2005). They showed dissociable patterns of resting-state functional connectivity, which closely resembled the ones we obtained by seeding directly in PFm, PGa and PF, respectively (Fig. 6D-F). By directly examining task-evoked activity in cytoarchitectonic areas (Fig. 4A), we confirm the functional distinctions between these cytoarchitectonic areas. Nelson et al. (2010) applied graph theory methods on resting-state and task-related fMRI data to define six distinct modules in lateral parietal cortex. This modularity referred to the left and not the right hemisphere, and provided comparatively less differentiation within the supramarginal gyrus, the anterior IPS or SPL (Nelson et al., 2010).

It is even more challenging to relate parietal parcellation in humans to that obtained in non-human primates (Mantini et al., 2012; Mars et al., 2011; Orban et al., 2006). Given the profound anatomical reorganizations that occurred in the parietal cortex during primate evolution (Van Essen and Dierker, 2007), it is possible that functions have shifted to areas that do not correspond topologically (Mantini et al., 2012). Some studies have tried to use resting-state connectivity or anatomical connectivity as a bridge between the two species (e.g., Mars et al., 2011). This provided evidence for a link between human area PF and monkey PFG (Gregoriou et al., 2006; Petrides and Pandya, 1984; Rozzi et al., 2006). Our data suggest that human PF, at least in the right hemisphere, shows spatially specific responses for an unattended but perceptually salient item in the display. Electrophysiological studies in monkeys have attributed this function to the rostral portion of area 7a, largely overlapping with monkey PFG (Constantinidis and Steinmetz, 2001a,b). Alternatively, human PF has been proposed to correspond to monkey

PF on the basis of their common involvement in action observation and understanding (Caspers et al., 2010; Nelissen et al., 2010; Rizzolatti and Arbib, 1998). PGa/PGp may correspond to monkey TPOc, based on a meta-analysis of deactivation studies in humans and macaques (Mantini et al., 2011). PFm has no obvious counterpart in the macaque brain (Caspers et al., 2011; Mars et al., 2011). The competition effect in hIP1 and hIP3 in the current study would imply that cytoarchitectonic areas hIP1 and hIP3 are possible homologues of LIP. We (Vandenberghe et al., 2005; Vandenberghe and Gillebert, 2009; Vandenberghe et al., 2012) and others (Grefkes and Fink, 2005; Sereno et al., 2001) have previously suggested that the IPS segment that is activated during the competition trials may correspond to the homologue of monkey LIP (Bisley and Goldberg, 2010). hIP3 may correspond, both structurally and functionally, to the ventral portion of monkey LIP (Bisley and Goldberg, 2003; Blatt et al., 1990; Liu et al., 2010). We have proposed that the middle segment of IPS, like monkey LIP (Bisley and Goldberg, 2010), plays a key role in the compilation of an attentional priority map (Gillebert et al., 2011, 2012a,b; Molenberghs et al., 2007, 2008; Vandenberghe et al., 2005; Vandenberghe and Gillebert, 2009; Vandenberghe et al., 2012). Further studies are warranted to establish the candidate monkey homologue of area PF and hIP1-3 in humans.

5 Conclusions

To conclude, the use of a cytoarchitectonic reference frame together with the combined study of spatial reorienting and attentional selection within the same experiment resolves the wide variability of activity foci within IPL associated with the invalidity effect: the invalidity map encompasses several cytoarchitectonic areas in the inferior parietal cortex. These areas however can be differentiated as a function of their functional specificity as well as their spatial pattern of functional connectivity. Attentional selection between competing stimuli and spatial reorienting are anatomically dissociable processes involving human cytoarchitectonic area hIP1/hIP3 and right PF, respectively. Several other bilateral areas in IPL, PFm, and PGa, show an invalidity effect but without the functional selectivity for attentional reorienting that is observed in right PF.

6 Acknowledgements

This work was supported by Research Foundation Flanders (FWO), Flanders, Belgium (grant number G0668.07 ESF EuroCores Program); Katholieke Universiteit Leuven (grant number OT/08/56) and Federaal Wetenschapsbeleid belspo (Inter-University Attraction Pole)(grant number P6/29). CRG is a PhD fellow, DM a postdoctoral fellow and RV a senior clinical investigator of the FWO.

References

Amunts, K., Zilles, K., 2001. Advances in cytoarchitectonic mapping of the human cerebral cortex. Neuroimaging Clin. N. Am. 11, 151–69.

Arrington, C.M., Carr, T.H., Mayer, A.R., Rao, S.M., 2000. Neural mechanisms of visual attention: object-based selection of a region in space. J. Cogn. Neurosci. 12, 106–117.

Ashburner, J., Friston, K.J., 2005. Unified segmentation. Neuroimage 26, 839–851.

Bays, P.M., Singh-Curry, V., Gorgoraptis, N., Driver, J., Husain, M., 2010. Integration of goal- and stimulus-related visual signals revealed by damage to human parietal cortex. J. Neurosci. Lett. 30, 5968–5978.

Beckmann, C.F., DeLuca, M., Devlin, J.T., Smith, S.M., 2005. Investigations into resting-state connectivity using independent component analysis. Philos. Trans. R. Soc. Lond. B Biol. Sci. 360, 1001–1013.

Binder, J.R., 2012. Task-induced deactivation and the "resting" state. Neuroimage 62, 1086–1091.

Bisley, J.W., Goldberg, M.E., 2003. Neuronal activity in the lateral intraparietal area and spatial attention. Science 299, 81–86.

Bisley, J.W., Goldberg, M.E., 2010. Attention, intention, and priority in the parietal lobe. Annu. Rev. Neurosci. 33, 1–21.

Blatt, G.J., Andersen, R.A., Stoner, G.R., 1990. Visual receptive field organization and cortico-cortical connections of the lateral intraparietal area (area LIP) in the macaque. J. Comp. Neurol. 299, 421–445.

Bressler, D.W., Silver, M.A., 2010. Spatial attention improves reliability of fMRI retinotopic mapping signals in occipital and parietal cortex. Neuroimage 53, 526–533.

Buckner, R.L., Andrews-Hanna, J.R., Schacter, D.L., 2008. The brain's default network: anatomy, function, and relevance to disease. Ann. N. Y. Acad. Sci. 1124, 1–38.

Bundesen, C., 1990. A Theory of Visual Attention. Psychol. Rev. 97, 523–547.

Caspers, S., Eickhoff, S.B., Geyer, S., Scheperjans, F., Mohlberg, H., Zilles, K., Amunts, K., 2008. The human inferior parietal lobule in stereotaxic space. Brain Struct. Funct. 212, 481–495.

Caspers, S., Eickhoff, S.B., Rick, T., von Kapri, A., Kuhlen, T., Huang, R., Shah, N.J., Zilles, K., 2011. Probabilistic fibre tract analysis of cytoarchitectonically defined human inferior parietal lobule areas reveals similarities to macaques. Neuroimage 58, 362–380.

Caspers, S., Geyer, S., Schleicher, A., Mohlberg, H., Amunts, K., Zilles, K., 2006. The human inferior parietal cortex: cytoarchitectonic parcellation and interindividual variability. Neuroimage 33, 430–448.

Caspers, S., Zilles, K., Laird, A.R., Eickhoff, S.B., 2010. ALE meta-analysis of action observation and imitation in the human brain. Neuroimage 50, 1148–1167.

Choi, H.J., Zilles, K., Mohlberg, H., Schleicher, A., Fink, G.R., Armstrong, E., Amunts, K., 2006. Cytoarchitectonic identification and probabilistic mapping of two distinct areas within the anterior ventral bank of the human intraparietal sulcus. J. Comp. Neurol. 495, 53–69.

Cohen, A.L., Fair, D.A., Dosenbach, N.U.F., Miezin, F.M., Dierker, D., Van Essen, D.C., Schlaggar, B.L., Petersen, S.E., 2008. Defining functional areas in individual human brains using resting functional connectivity MRI. Neuroimage 41, 45–57.

Constantinidis, C., Steinmetz, M.A., 2001a. Neuronal responses in area 7a to multiple-stimulus displays: I. Neurons encode the location of the salient stimulus. Cereb. Cortex 11, 581–591.

Constantinidis, C., Steinmetz, M.A., 2001b. Neuronal responses in area 7a to multiple stimulus displays: II. Responses are suppressed at the cued location. Cereb. Cortex 11, 592–597.

Corbetta, M., Kincade, J., Ollinger, J., Mcavoy, M., Shulman, G., 2000. Voluntary orienting is dissociated from target detection in human posterior parietal cortex. Nat. Neurosci. 3, 292–297.

Corbetta, M., Kincade, M.J., Lewis, C.L., Snyder, A.Z., Sapir, A., 2005. Neural basis and recovery of spatial attention deficits in spatial neglect. Nat. Neurosci. 8, 1603–1610.

Corbetta, M., Miezin, F., Shulman, G., Petersen, S., 1993. A PET study of visuospatial attention. J. Neurosci. 13, 1202–1226.

Corbetta, M., Patel, G., Shulman, G.L., 2008. The reorienting system of the human brain: from environment to theory of mind. Neuron 58, 306–324.

Corbetta, M., Shulman, G., 2002. Control of goal-directed and stimulus-driven attention in the brain. Nat. Rev. Neurosci. 3, 201–215.

Corbetta, M., Shulman, G.L., 2011. Spatial neglect and attention networks. Annu. Rev. Neurosci. 34, 569–599.

Decety, J., Lamm, C., 2007. The role of the right temporoparietal junction in social interaction: how low-level computational processes contribute to meta-cognition. Neuroscientist 13, 580–593.

Desimone, R., Duncan, J., 1995. Neural mechanisms of selective visual attention. Annu. Rev. Neurosci. 18, 193–222.

Downar, J., Crawley, A.P., Mikulis, D.J., Davis, K.D., 2000. A multimodal cortical network for the detection of changes in the sensory environment. Nat. Neurosci. 3, 277–283.

Duncan, J., 2010. The multiple-demand (MD) system of the primate brain: mental programs for intelligent behaviour. Trends Cogn. Sci. 14, 172–179.

Ebisch, S.J.H., Gallese, V., Willems, R.M., Mantini, D., Groen, W.B., Romani, G.L., Buitelaar, J.K., Bekkering, H., 2011. Altered intrinsic functional connectivity of anterior and posterior insula regions in high-functioning participants with autism spectrum disorder. Hum. Brain Mapp. 32, 1013–1028.

Eickhoff, S.B., Heim, S., Zilles, K., Amunts, K., 2006. Testing anatomically specified hypotheses in functional imaging using cytoarchitectonic maps. Neuroimage 32, 570–582.

Eickhoff, S.B., Paus, T., Caspers, S., Grosbras, M.H., Evans, A.C., Zilles, K., Amunts, K., 2007. Assignment of functional activations to probabilistic cytoarchitectonic areas revisited. Neuroimage 36, 511–521.

Eickhoff, S.B., Stephan, K.E., Mohlberg, H., Grefkes, C., Fink, G.R., Amunts, K., Zilles, K., 2005. A new SPM toolbox for combining probabilistic cytoarchitectonic maps and functional imaging data. Neuroimage 25, 1325–1335.

Everitt, B.S., Landau, S., Leese, M., 2001. Cluster Analysis. Hodder Arnold, London.

Felleman, D.J., Van Essen, D.C., 1991. Distributed hierarchical processing in the primate cerebral cortex. Cereb. Cortex 1, 1–47.

Fox, M.D., Corbetta, M., Snyder, A.Z., Vincent, J.L., Raichle, M.E., 2006. Spontaneous neuronal activity distinguishes human dorsal and ventral attention systems. Proc. Natl. Acad. Sci. U. S. A. 103, 10046–10051.

Fox, M.D., Snyder, A.Z., Vincent, J.L., Corbetta, M., Essen, D.C.V., Raichle, M.E., 2005. The human brain is intrinsically organized into dynamic, anticorrelated functional networks. Proc. Natl. Acad. Sci. U. S. A. 102, 9673–9678.

Giesbrecht, B., Woldorff, M.G., Song, A.W., Mangun, G.R., 2003. Neural mechanisms of top-down control during spatial and feature attention. Neuroimage 19, 496–512.

Gillebert, C.R., Caspari, N., Wagemans, J., Peeters, R., Dupont, P., Vandenberghe, R., 2012a. Spatial stimulus configuration and attentional selection: extrastriate and superior parietal interactions. Cereb. Cortex In press.

Gillebert, C.R., Dyrholm, M., Vangkilde, S., Kyllingsbæk, S., Peeters, R., Vandenberghe, R., 2012b. Attentional priorities and access to short-term memory: Parietal interactions. Neuroimage 62, 1551–1562.

Gillebert, C.R., Mantini, D., Thijs, V., Sunaert, S., Dupont, P., Vandenberghe, R., 2011. Lesion evidence for the critical role of the intraparietal sulcus in spatial attention. Brain 134, 1694–1709.

Grefkes, C., Fink, G., 2005. The functional organization of the intraparietal sulcus in humans and monkeys. J. Anat. 207, 3–17.

Gregoriou, G.G., Borra, E., Matelli, M., Luppino, G., 2006. Architectonic organization of the inferior parietal convexity of the macaque monkey. J. Comp. Neurol. 496, 422–451.

Greicius, M.D., Krasnow, B., Reiss, A.L., Menon, V., 2003. Functional connectivity in the resting brain: a network analysis of the default mode hypothesis. Proc. Natl. Acad. Sci. U. S. A. 100, 253–258.

Hayes, D.J., Huxtable, A.G., 2012. Interpreting deactivations in neuroimaging. Front. Psychol. 3, 27.

Hopfinger, J.B., Buonocore, M.H., Mangun, G.R., 2000. The neural mechanisms of top-down attentional control. Nat. Neurosci. 3, 284–291.

Juch, H., Zimine, I., Seghier, M.L., Lazeyras, F., Fasel, J.H.D., 2005. Anatomical variability of the lateral frontal lobe surface: implication for intersubject variability in language neuroimaging. Neuroimage 24, 504–514.

Kastner, S., Pinsk, M.A., Weerd, P.D., Desimone, R., Ungerleider, L.G., 1999. Increased activity in human visual cortex during directed attention in the absence of visual stimulation. Neuron 22, 751–761.

Kelley, T.A., Serences, J.T., Giesbrecht, B., Yantis, S., 2008. Cortical mechanisms for shifting and holding visuospatial attention. Cereb. Cortex 18, 114–125.

Kim, Y.H., Gitelman, D.R., Nobre, A.C., Parrish, T.B., LaBar, K.S., Mesulam, M.M., 1999. The large-scale neural network for spatial attention displays multifunctional overlap but differential asymmetry. Neuroimage 9, 269–277.

Kincade, J.M., Abrams, R.A., Astafiev, S.V., Shulman, G.L., Corbetta, M., 2005. An event-related functional magnetic resonance imaging study of voluntary and stimulus-driven orienting of attention. J. Neurosci. 25, 4593–4604.

Lachaux, J.P., Jung, J., Mainy, N., Dreher, J.C., Bertrand, O., Baciu, M., Minotti, L., Hoffmann, D., Kahane, P., 2008. Silence is golden: transient neural deactivation in the prefrontal cortex during attentive reading. Cereb. Cortex 18, 443–450.

Liu, Y., Yttri, E.A., Snyder, L.H., 2010. Intention and attention: different functional roles for LIPd and LIPv. Nat. Neurosci. 13, 495–500.

MacMillan, N., Creelman, C., 1991. Detection Theory: A User's Guide. Cambridge University Press, Cambridge, UK.

Mantini, D., Gerits, A., Nelissen, K., Durand, J.B., Joly, O., Simone, L., Sawamura, H., Wardak, C., Orban, G.A., Buckner, R.L., Vanduffel, W., 2011. Default mode of brain function in monkeys. J. Neurosci. 31, 12954–12962.

Mantini, D., Hasson, U., Betti, V., Perrucci, M.G., Romani, G.L., Corbetta, M., Orban, G.A., Vanduffel, W., 2012. Interspecies activity correlations reveal functional correspondence between monkey and human brain areas. Nat. Methods 9, 277–282.

Mantini, D., Perrucci, M.G., Gratta, C.D., Romani, G.L., Corbetta, M., 2007. Electrophysiological signatures of resting state networks in the human brain. Proc. Natl. Acad. Sci. U. S. A. 104, 13170–13175.

Mantini, D., Vanduffel, W., 2012. Emerging roles of the brain's default network. Neuroscientist .

Mars, R.B., Jbabdi, S., Sallet, J., O'Reilly, J.X., Croxson, P.L., Olivier, E., Noonan, M.P., Bergmann, C., Mitchell, A.S., Baxter, M.G., Behrens, T.E.J., Johansen-Berg, H., Tomassini, V., Miller, K.L., Rushworth, M.F.S., 2011. Diffusion-weighted imaging tractography-based parcellation of the human parietal cortex and comparison with human and macaque resting-state functional connectivity. J. Neurosci. 31, 4087–4100.

Mars, R.B., Sallet, J., Schüffelgen, U., Jbabdi, S., Toni, I., Rushworth, M.F.S., 2012. Connectivity-based subdivisions of the human right "temporoparietal junction area": Evidence for different areas participating in different cortical networks. Cereb. Cortex 22, 1894–903.

McKiernan, K.A., Kaufman, J.N., Kucera-Thompson, J., Binder, J.R., 2003. A parametric manipulation of factors affecting task-induced deactivation in functional neuroimaging. J. Cogn. Neurosci. 15, 394–408.

Molenberghs, P., Gillebert, C.R., Peeters, R., Vandenberghe, R., 2008. Convergence between lesion-symptom mapping and functional magnetic resonance imaging of spatially selective attention in the intact brain. J. Neurosci. 28, 3359–3373.

Molenberghs, P., Mesulam, M.M., Peeters, R., Vandenberghe, R., 2007. Re-mapping attentional priorities: Differential contribution of superior parietal lobule and intraparietal sulcus. Cereb. Cortex 17, 2703–2712.

Nardo, D., Santangelo, V., Macaluso, E., 2011. Stimulus-driven orienting of visuo-spatial attention in complex dynamic environments. Neuron 69, 1015–1028.

Nelissen, N., Pazzaglia, M., Vandenbulcke, M., Sunaert, S., Fannes, K., Dupont, P., Aglioti, S.M., Vandenberghe, R., 2010. Gesture discrimination in primary progressive aphasia: the intersection between gesture and language processing pathways. J. Neurosci. 30, 6334–6341.

Nelson, S.M., Cohen, A.L., Power, J.D., Wig, G.S., Miezin, F.M., Wheeler, M.E., Velanova, K., Donaldson, D.I., Phillips, J.S., Schlaggar, B.L., Petersen, S.E., 2010. A parcellation scheme for human left lateral parietal cortex. Neuron 67, 156–170.

Nobre, A.C., Sebestyen, G.N., Gitelman, D.R., Mesulam, M.M., Frackowiak, R.S., Frith, C.D., 1997. Functional localization of the system for visuospatial attention using positron emission tomography. Brain 120, 515–533.

Orban, G.A., Claeys, K., Nelissen, K., Smans, R., Sunaert, S., Todd, J.T., Wardak, C., Durand, J.B., Vanduffel, W., 2006. Mapping the parietal cortex of human and non-human primates. Neuropsychologia 44, 2647–2667.

Orban, G.A., Vanduffel, W., 2007. Comment on devlin and poldrack. Neuroimage 37, 1057–8;.

Petrides, M., Pandya, D., 1984. Projections to the frontal cortex from the posterior parietal region in the rhesus monkey. J. Comp. Neurol. 228, 105–116.

Posner, M.I., 2012. Cognitive Neuroscience of Attention. The Guilford Press, New York / London.

Posner, M.I., Snyder, C.R., Davidson, B.J., 1980. Attention and the detection of signals. J. Exp. Psychol. 109, 160–174.

Posner, M.I., Walker, J.A., Friedrich, F.J., Rafal, R.D., 1984. Effects of parietal injury on covert orienting of attention. J. Neurosci. 4, 1863–1874.

Pravatà, E., Sestieri, C., Mantini, D., Briganti, C., Colicchio, G., Marra, C., Colosimo, C., Tartaro, A., Romani, G.L., Caulo, M., 2011. Functional connectivity MR imaging of the language network in patients with drug-resistant epilepsy. AJNR. Am. J. Neuroradiol. 32, 532–540.

Rafal, R., 1998. Neglect. In: Parasuraman, R. (Ed.), The attentive brain The MIT Press, Cambridge MA, pp.489–525.

Rizzolatti, G., Arbib, M.A., 1998. Language within our grasp. Trends Neurosci 21, 188–194.

Rosenberg-Lee, M., Chang, T.T., Young, C.B., Wu, S., Menon, V., 2011. Functional dissociations between four basic arithmetic operations in the human posterior parietal cortex: a cytoarchitectonic mapping study. Neuropsychologia 49, 2592–2608.

Rozzi, S., Calzavara, R., Belmalih, A., Borra, E., Gregoriou, G.G., Matelli, M., Luppino, G., 2006. Cortical connections of the inferior parietal cortical convexity of the macaque monkey. Cereb. Cortex 16, 1389–1417.

Rushworth, M.F.S., Behrens, T.E.J., Johansen-Berg, H., 2006. Connection patterns distinguish 3 regions of human parietal cortex. Cereb. Cortex 16, 1418–1430.

Scheperjans, F., Eickhoff, S.B., Höke, L., Mohlberg, H., Hermann, K., Amunts, K., Zilles, K., 2008a. Probabilistic maps, morphometry, and variability of cytoarchitectonic areas in the human superior parietal cortex. Cereb. Cortex 18, 2141–2157.

Scheperjans, F., Hermann, K., Eickhoff, S.B., Amunts, K., Schleicher, A., Zilles, K., 2008b. Observer-independent cytoarchitectonic mapping of the human superior parietal cortex. Cereb. Cortex 18, 846–867.

Schleicher, A., Amunts, K., Geyer, S., Morosan, P., Zilles, K., 1999. Observer-independent method for microstructural parcellation of cerebral cortex: A quantitative approach to cytoarchitectonics. Neuroimage 9, 165–177.

Seeley, W.W., Menon, V., Schatzberg, A.F., Keller, J., Glover, G.H., Kenna, H., Reiss, A.L., Greicius, M.D., 2007. Dissociable intrinsic connectivity networks for salience processing and executive control. J. Neurosci. 27, 2349–2356.

Seghier, M.L., Lazeyras, F., Pegna, A.J., Annoni, J.M., Khateb, A., 2008. Group analysis and the subject factor in functional magnetic resonance imaging: analysis of fifty right-handed healthy subjects in a semantic language task. Hum. Brain Mapp. 29, 461–477.

Sereno, M.I., Pitzalis, S., Martinez, A., 2001. Mapping of contralateral space in retinotopic coordinates by a parietal cortical area in humans. Science 294, 1350–1354.

Shulman, G.L., Astafiev, S.V., McAvoy, M.P., d'Avossa, G., Corbetta, M., 2007. Right TPJ deactivation during visual search: functional significance and support for a filter hypothesis. Cereb. Cortex 17, 2625–2633.

Silver, M.A., Kastner, S., 2009. Topographic maps in human frontal and parietal cortex. Trends Cogn. Sci. 13, 488–495.

Silver, M.A., Ress, D., Heeger, D.J., 2005. Topographic maps of visual spatial attention in human parietal cortex. J. Neurophysiol. 94, 1358–1371.

Skudlarski, P., Jagannathan, K., Calhoun, V.D., Hampson, M., Skudlarska, B.A., Pearlson, G., 2008. Measuring brain connectivity: diffusion tensor imaging validates resting state temporal correlations. Neuroimage 43, 554–561.

Slotnick, S.D., Schwarzbach, J., Yantis, S., 2003. Attentional inhibition of visual processing in human striate and extrastriate cortex. Neuroimage 19, 1602–1611.

Swisher, J.D., Halko, M.A., Merabet, L.B., McMains, S.A., Somers, D.C., 2007. Visual topography of human intraparietal sulcus. J. Neurosci. 27, 5326–5337.

Uddin, L.Q., Supekar, K., Amin, H., Rykhlevskaia, E., Nguyen, D.A., Greicius, M.D., Menon, V., 2010. Dissociable connectivity within human angular gyrus and intraparietal sulcus: evidence from functional and structural connectivity. Cereb. Cortex 20, 2636–2646.

Van Essen, D.C., 2005. A Population-Average, Landmark- and Surface-based (PALS) atlas of human cerebral cortex. Neuroimage 28, 635–662.

Van Essen, D.C., Dierker, D.L., 2007. Surface-based and probabilistic atlases of primate cerebral cortex. Neuron 56, 209–225.

Vandenberghe, R., Geeraerts, S., Molenberghs, P., Lafosse, C., Vandenbulcke, M., Peeters, K., Peeters, R., Hecke, P.V., Orban, G., 2005. Attentional responses to unattended stimuli in human parietal cortex. Brain 128, 2843–2857.

Vandenberghe, R., Gillebert, C.R., 2009. Parcellation of parietal cortex: convergence between lesion-symptom mapping and mapping of the intact functioning brain. Behav. Brain Res. 199, 171–182.

Vandenberghe, R., Gitelman, D.R., Parrish, T.B., Mesulam, M.M., 2001. Functional specificity of superior parietal mediation of spatial shifting. Neuroimage 14, 661–673.

Vandenberghe, R., Molenberghs, P., Gillebert, C.R., 2012. Spatial attention deficits in humans: The critical role of superior compared to inferior parietal lesions. Neuropsychologia 50, 1091–1103.

Vossel, S., Thiel, C.M., Fink, G.R., 2006. Cue validity modulates the neural correlates of covert endogenous orienting of attention in parietal and frontal cortex. Neuroimage 32, 1257–1264.

Wager, T.D., Nichols, T.E., 2003. Optimization of experimental design in fMRI: a general framework using a genetic algorithm. Neuroimage 18, 293–309.

Wandell, B., Dumoulin, S., Brewer, A., 2007. Visual field maps in human cortex. Neuron 56, 366–383.

Woldorff, M.G., Hazlett, C.J., Fichtenholtz, H.M., Weissman, D.H., Dale, A.M., Song, A.W., 2004. Functional parcellation of attentional control regions of the brain. J. Cogn. Neurosci. 16, 149–165.

Wu, S.S., Chang, T.T., Majid, A., Caspers, S., Eickhoff, S.B., Menon, V., 2009. Functional heterogeneity of inferior parietal cortex during mathematical cognition assessed with cytoarchitectonic probability maps. Cereb. Cortex 19, 2930–2945.

Yantis, S., Schwarzbach, J., Serences, J.T., Carlson, R.L., Steinmetz, M.A., Pekar, J., Courtney, S.M., 2002. Transient neural activity in human parietal cortex during spatial attention shifts. Nat. Neurosci. 5, 995–1003.

Zilles, K., Schleicher, A., Palomero-Gallagher, N., Amunts, K., 2002. Quantitative analysis of cyto- and receptor architecture of the human brain. In: Mazziotta, J., Toga, A. (Eds.), Brain Mapping, the Methods Elsevier, pp. 573–602.